Theoretical Analysis of Optical Absorption Spectra of Parallel Nanowire Dimers and Dolmen Trimers

Pratima Pandeya[a] and Christine M. Aikens[a,*]

a) Department of Chemistry, Kansas State University, Manhattan, KS 66506, USA
* cmaikens@ksu.edu; 1-785-532-0954

ABSTRACT

Plasmonic nanoparticles are well known for their properties of electromagnetic field enhancement and surface spectroscopy enhancement. We used the plasmon hybridization method and group theory to study parallel dimers and dolmen trimers of Ag_n (n = 4, 6, 10) nanoparticles. Interactions between the plasmon modes were studied with decreasing inter-particle separation distances. Time dependent density functional calculations are performed on the structures using the BP86/DZ level of theory. In dimers, the decrease of the inter-particle separation blue-shifts the longitudinal peak but the transverse peak position is not affected significantly. In trimers, a new peak is also observed as a shoulder of the longitudinal peak. When the inter-particle separation reduces to 0.6 nm in dimers and trimers, a new peak emerges between the longitudinal and transverse peaks. This new peak red-shifts and increases in intensity upon further decreasing the inter-particle separation. Analysis of the transition densities and symmetries for the respective peaks shows that the new peak arises from a charge-transfer excitation.

1. INTRODUCTION

A localized surface plasmon resonance is a collective oscillation of free electrons in metallic nanoparticles upon interaction with electromagnetic radiation. The oscillation frequency depends on the shape, size and dielectric environment of the nanoparticles.[1] Plasmonic nanoparticles are of great interest as they enhance the local electromagnetic fields and are very important for surface spectroscopy.[2] Experiments have shown enhancements as large as 10−14 orders of magnitude, enabling spectroscopic detection of a single molecule.[3-5] Different shapes of nanoparticles have been studied such as nano shells,[6-7] rods,[8-9] disks,[10] cubes,[11] cylinders,[12] triangles[13] and rings.[14] Among them, cylindrical nanowires and nanorods have received a lot of interest because their optical properties are very sensitive to their aspect ratio.[15-17] Arrays of nanoparticles are ideal for different applications like biosensing,[18-19] nanolasing,[20] spectroscopy[21-22] and as optical waveguides.[23-25] In consequence, a number of interesting studies have been performed on ordered arrays of nanoparticles[26-34] such as dolmen trimers[35-38] and end-to-end and side-by-side arrangements of nanorods.[39-44]

The optical properties of nanoparticle assemblies are dramatically influenced by the coupling of the plasmon resonances of nearby nanoparticles. Symmetry breaking often accompanies formation of nanoparticle assemblies, and the nanoparticle coupling leads to different bright and dark modes.[45] Plasmonic modes of individual particles hybridize to form new collective modes in multiparticle systems.[46] Plasmon coupling has advantages in surface-enhanced Raman scattering (SERS)[47] and tip-enhanced Raman scattering.[48] Nanoparticle dimers are the most versatile and simple multiparticle structures studied so far. Many experimental and theoretical studies have already been performed on nanoparticle homo and hetero-dimers.[49-55] Dimers have found applications ranging from sensing and spectroscopy[46, 56] to nonlinear optics.[57]

Nordlander and Prodan have developed a plasmon hybridization model[58] that helps to elucidate the plasmon resonances present in an array of nanostructures. This approach is similar to the interaction of atomic orbitals to form molecular orbitals; the plasmon modes of the constituent nanoparticles hybridize to form composite plasmon modes. Plasmons of composite nanoparticles can thus be described as bonding and antibonding combinations arising from hybridization of the individual nanoparticle plasmons. The method has been used successfully to describe the plasmon resonances in concentric spherical metallic nanoparticles,[59] nanoparticle dimers,[60] and various other geometries like nanoshell, nanoeggs, nanomatryushkas, nanorice, nanoparticle trimers, nanoparticle quadrumers, and a semi-infinite surface or a metallic film.[61]

Numerous studies examine nanoparticles in close proximity.[39, 62-72] The most widely used approach for analyzing excitation energy transfer in nanoparticle assemblies involves classical methods such as finite difference time domain (FDTD)[73-74] calculations or similar methods based on solving Maxwell's equations.[25, 73, 75-76] But, because quantum effects play a major role when small inter-particle dimensions are present, researchers have proposed quantum-corrected models to the classical electro-magnetic simulations for these systems.[77-78] Several studies have shown that classical electrodynamics simulations fail for small nanoparticles and nanoparticle assemblies with small separations.[46, 78-81] As these models do not give an atomistic treatment of the systems, quantum mechanical methods such as density functional theory (DFT) are essential to predict the quantum effects at small separation distances. In consequence, studies have been performed on nanoparticle assemblies using quantum mechanical methods. Quantum effects such as surface scattering, electron spill-out at the surface, coupling of plasmons to single particle excitations and the nonlocality of electronic response play a dominant role for nano sized structures.[79, 82] A quantum mechanical study can give a realistic description of the overlap and tunneling of plasmons for closely separated nanoparticles.[83-84] Tunneling breaks down the local field enhancement predicted by classical theory at the subnanometer regime and leads to the formation of a charge transfer plasmon.[65, 78, 85-86] A charge transfer plasmon is observed where there is direct charge transfer from one nanoparticle to another, when the nanoparticles touch each other, or when a conductive junction is established between them.[87-88] Savage et al. used a quantum corrected model to predict the onset of quantum tunneling effects at around 0.3 nm particle separation.[81] They have shown that the quantum regime starts with a blue shift of hybridized modes in coupled nanoparticles. Zhang et al. showed that the atomic structure of the metal clusters plays a key role in determining accurately both the absorption cross section and electric field enhancement and the effect is more critical when the distance between the nanoparticles is smaller than around 0.3 nm[89] which is also discussed in the review article by Varas et al.[90]

In this paper, we investigate small silver nanowires, their dimers (parallel side-by-side arrangement) and trimers (dolmen structure). We use a quantum mechanical time-dependent density functional theory (TDDFT)[91] method that offers the possibility to address the optical response of plasmonic systems at the fully quantum ab initio level. Although these nanowires are small, the excitations in similar nanowire systems have previously been shown to be plasmonic using approaches that scale e.g. the electron-electron interactions.[92-93] We look into the evolution of the optical absorption spectra of silver nanowire dimers and trimers with different monomer lengths and changing inter-particle distances. We use group theory considerations and the plasmon hybridization method to explain the origin of a new peak in the optical absorption spectra of the nanowire assemblies with decreasing inter-particle distance. We also examine the transition electron densities in dimers and trimers and show that these transition densities are very helpful to describe the evolution of new peaks in the absorption spectra with the decrease in inter-particle

separation. The study of these nanowire assemblies is important to understand the mechanism of interaction of plasmons in composite systems.

2. COMPUTATIONAL DETAILS

All calculations are performed with the Amsterdam Density Functional (ADF)[94] 2017 package. Geometry optimizations on the monomer nanowires are performed with linear symmetry using the generalized gradient approximation (GGA) Becke–Perdew (BP86)[95-97] exchange-correlation functional with a large frozen core double-zeta (DZ) basis set; the optimized coordinates are provided in Table S1. It should be noted that these geometries do not represent global minima, but are useful model systems for understanding the properties of larger nanorods. Scalar relativistic effects are included with the zeroth-order regular approximation (ZORA).[98] Excitation spectra are calculated using linear response time-dependent density functional theory (TDDFT).[99-102] Unless otherwise noted, the exchange correlation functional used for the TDDFT calculations is the Perdew-Burke-Ernzerhof (PBE) GGA.[103] Time dependent Hartree Fock (TDHF)[104-105] calculations are also carried out on dimers and trimers in order to analyze the charge transfer plasmon. The absorption spectra are convoluted with a Gaussian with a full width at half maximum (FWHM) of 0.2 eV. Multiple excited states may contribute to each plasmon peak; each excited state may be expressed as a linear combination of excited determinants, where each excited determinant can be expressed as an occupied-to-virtual orbital transition. Transition electron densities are computed, which determine how electron density changes between the ground state and an excited state. Orbitals are represented in the ADF-GUI with a contour value of 0.02 and the transition density plots are obtained with an iso-value of 0.02 unless otherwise stated.

The monomers, dimers and trimers of Ag_4, Ag_6 and Ag_{10} nanowires are studied at different inter-particle distances. For dimers, the two monomers are arranged in a side-to-side fashion to form a dimer with D_{2h} symmetry. For trimers, the third monomer is placed on the top of dimer to form a dolmen structure with C_{2v} symmetry. The structures of the studied assemblies of nanowires are shown in Figure 1. Only homo-dimers and homo-trimers are considered in this work. To construct these structures, we set the monomers at separation distances (d) of 2 nm, 1.5 nm, 1 nm, 0.9 nm, 0.8 nm, 0.7 nm, 0.6 nm, 0.55 nm, 0.5 nm, 0.45 nm, and 0.4 nm from each other.

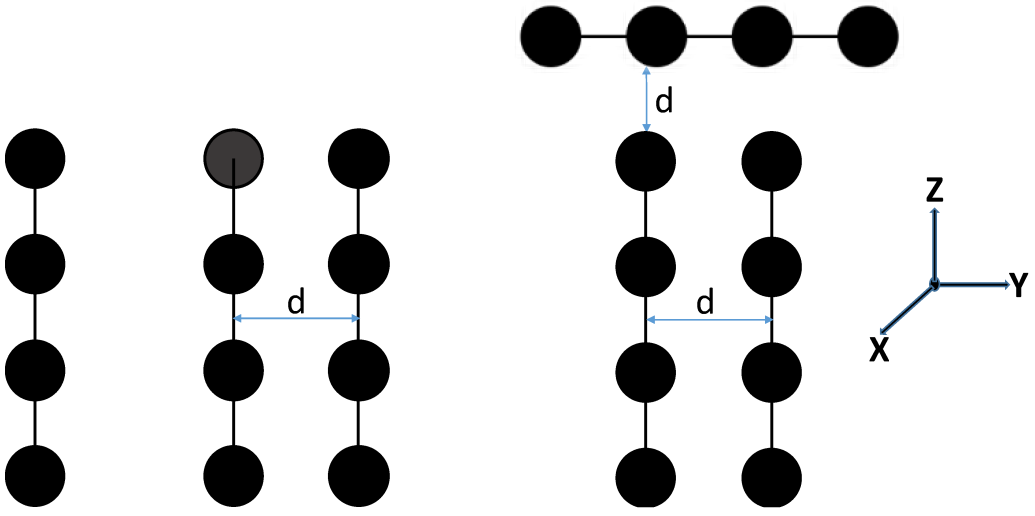

Figure 1. Nanowires assemblies examined in this work: monomer, parallel dimer, and dolmen trimer.

3. RESULTS AND DISCUSSION

We first consider the absorption spectra of Ag_n (n = 4, 6, 10) monomers, then discuss the absorption spectra of dimers and trimers. We look in detail into the changes in absorption spectra with the change of aspect ratio for the monomers and also with respect to the change in monomer separation distance for the dimers and trimers. Then, we study the main transitions, symmetry representations and types of orbitals corresponding to the main absorption peaks of the monomers, dimers, and trimers. We also examine the transition electron densities to describe the observed spectral behavior.

3.1 Absorption spectra for monomers of Ag_n (n = 4, 6, 10)

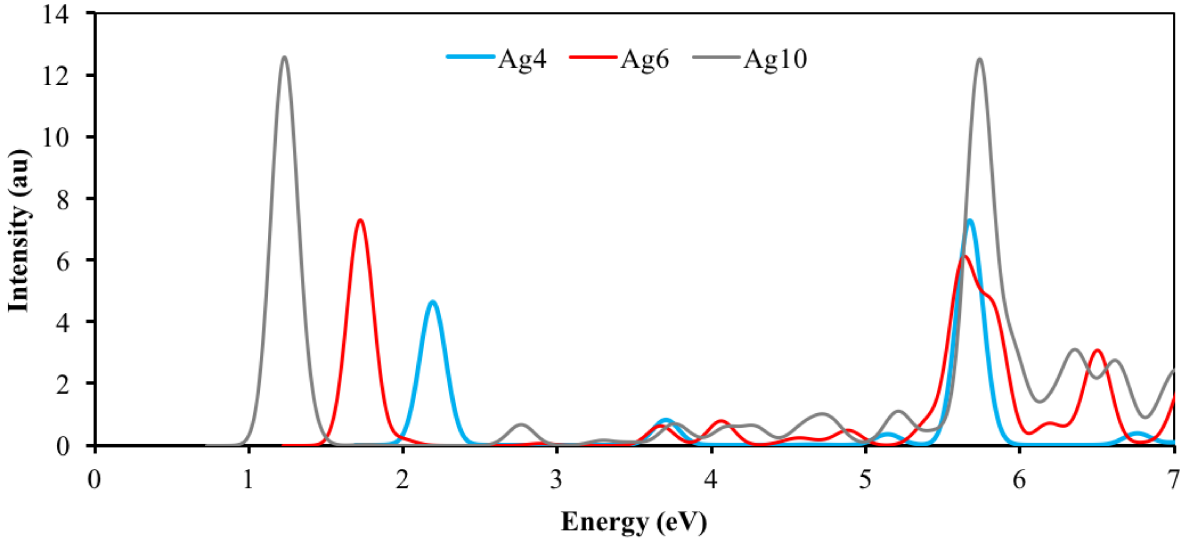

Figure 2. Absorption spectra for Ag_4, Ag_6 and Ag_{10} monomer nanowires.

As shown in Figure 2, nanowire monomers exhibit two major peaks in their absorption spectra. The sharp peak at lower energies is the longitudinal peak which arises mainly from plasmon oscillation along the long axis of nanowires. This peak originates from the HOMO → LUMO transition and has Σ_u symmetry. These orbitals can also be represented as Σ_n, in which n represents the axial quantum number of the orbital (i.e. the number of axial nodes + 1) as if it were a delocalized particle-in-a-cylinder orbital.[106] The main transitions and the orbitals involved in the longitudinal peak of nanowire monomers are shown in Table 1. $\Sigma_n \rightarrow \Sigma_{n+1}$ transitions are primarily responsible for the longitudinal peak in all nanowire monomers. The shapes of the orbitals that contribute to the longitudinal peak of the Ag_4, Ag_6 and Ag_{10} nanowires are shown in Figure 3. The intensity of the longitudinal peak increases from Ag_4 to Ag_{10} (Figure 2) as determined by the increasing oscillator strength of the state responsible for this peak (Table 1). This is due to the increase in the number of electrons with the increase in system size, which causes a stronger plasmon oscillation.[106] This linear increase of oscillator strength with the chain length has also been observed in previous studies.[107] Note that the signs associated with the transition dipole moments in Tables 1 and 2 are the signs printed in the TDDFT calculations, so the absolute signs

do not matter for a given system; however, within a given excitation, the relative signs are meaningful for different contributions to the excitation.

Table 1. Main transitions, excited state energies, oscillator strengths, and transition dipole moments for the longitudinal peak of monomer nanowires.

Nanowire	Transitions (Symmetry representation)	Transitions (Delocalized orbital notation)	Energy (eV)	Oscillator Strength (a.u.)	Transition Dipole Moment (a.u.)
Ag_4	$3\sigma_u \rightarrow 4\sigma_g$	$\Sigma_2 \rightarrow \Sigma_3$	2.19	0.99	-4.82
Ag_6	$5\sigma_g \rightarrow 5\sigma_u$	$\Sigma_3 \rightarrow \Sigma_4$	1.72	1.55	6.46
Ag_{10}	$8\sigma_g \rightarrow 8\sigma_u$	$\Sigma_5 \rightarrow \Sigma_6$	1.23	2.61	-9.48

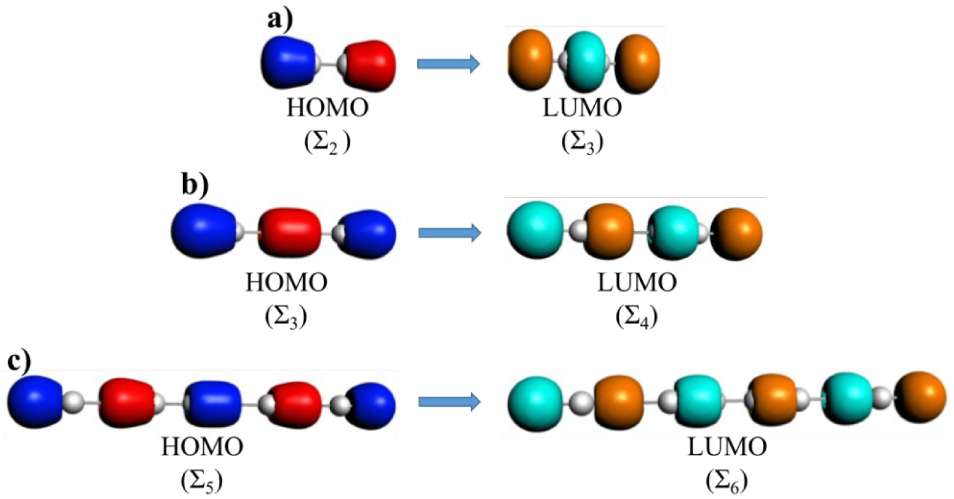

Figure 3. Orbitals primarily responsible for the longitudinal peak of a) Ag_4, b) Ag_6 and c) Ag_{10} nanowires.

On comparing the monomer spectra of different chain lengths (Figure 2), the longitudinal peak is seen to be sensitive to aspect ratio of the nanowire which was also observed in previous studies.[108] This peak shows a significant redshift as the length of the wire chain increases from Ag_4 to Ag_{10}. This behavior can be explained in accordance with the particle-in-a-cylinder model, which demonstrates why a linear relationship between the aspect ratio of the nanowire (which is proportional to nanowire length for a given nanowire diameter) and the longitudinal plasmon wavelength is typically observed.[106]

The peak at higher energy in the absorption spectra is the transverse peak. It arises due to the plasmon oscillation along the short axis of nanowire and exhibits Π_u symmetry. The transverse peak arises mainly from transitions between Σ and Π levels of the nanowires as shown in Figure 4 for the Ag_4 nanowire. Our results on the study of longitudinal and transverse peaks of monomers match with the previous studies on nanowires[107, 109-110] and are included in this paper for the purpose of completeness. The transverse peak is broader compared to the longitudinal peak as it involves multiple $\Sigma \rightarrow \Pi$ transitions, each with lower dipole moment contributions compared to the longitudinal peak, as shown in Tables 1 and 2. Transition dipole moments increase as the length of nanowire increases. An absorption spectrum for the Ag_6 monomer is shown in Figure S1 which

clearly shows the multiple transitions involved in the transverse peak and a single strong transition for longitudinal peak. The main transitions and the types of orbitals involved for transverse peak of the monomers are shown in Table 2. The change of aspect ratio has a negligible effect on the transverse peak position (Figure 2).

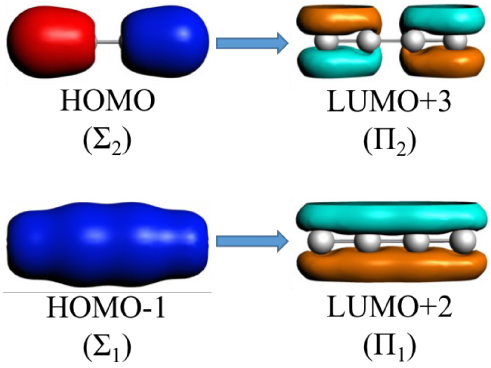

Figure 4. Orbitals primarily responsible for the transverse peak of the Ag_4 nanowire.

Table 2. Energies, oscillator strengths, main transitions, and transition dipole moments for the transverse peak of monomer nanowires.

Nanowire	Energy (eV)	Oscillator Strength (a.u.)	Transitions (Symmetry representation)	Transitions (Delocalized orbital notation)	Transition Dipole Moment (a.u.)
Ag_4	5.67	0.76	$3\sigma_u \rightarrow 3\pi_g$	$\Sigma_2 \rightarrow \Pi_2$	-1.65
			$3\sigma_g \rightarrow 3\pi_u$	$\Sigma_1 \rightarrow \Pi_1$	-1.45
Ag_6	5.62	0.57	$5\sigma_g \rightarrow 5\pi_u$	$\Sigma_3 \rightarrow \Pi_3$	1.11
			$4\sigma_u \rightarrow 4\pi_g$	$\Sigma_2 \rightarrow \Pi_2$	1.00
			$4\sigma_g \rightarrow 4\pi_u$	$\Sigma_1 \rightarrow \Pi_1$	0.86
			$2\pi_u \rightarrow 6\sigma_g$	d-band $\rightarrow \Sigma_5$	-0.28
	5.74	0.14	$5\sigma_g \rightarrow 5\pi_u$	$\Sigma_3 \rightarrow \Pi_3$	0.47
			$4\sigma_u \rightarrow 4\pi_g$	$\Sigma_2 \rightarrow \Pi_2$	0.62
			$4\sigma_g \rightarrow 4\pi_u$	$\Sigma_1 \rightarrow \Pi_1$	0.19
			$4\sigma_g \rightarrow 5\pi_u$	$\Sigma_1 \rightarrow \Pi_3$	-0.13
	5.84	0.38	$5\sigma_g \rightarrow 5\pi_u$	$\Sigma_3 \rightarrow \Pi_3$	0.78
			$4\sigma_u \rightarrow 4\pi_g$	$\Sigma_2 \rightarrow \Pi_2$	0.57
			$4\sigma_g \rightarrow 4\pi_u$	$\Sigma_1 \rightarrow \Pi_1$	0.64
			$2\pi_u \rightarrow 6\sigma_g$	d-band $\rightarrow \Sigma_5$	0.32
Ag_{10}	5.74	1.22	$8\sigma_g \rightarrow 8\pi_u$	$\Sigma_5 \rightarrow \Pi_5$	1.03
			$7\sigma_u \rightarrow 7\pi_g$	$\Sigma_4 \rightarrow \Pi_4$	0.87
			$7\sigma_g \rightarrow 7\pi_u$	$\Sigma_3 \rightarrow \Pi_3$	0.84
			$6\sigma_u \rightarrow 6\pi_g$	$\Sigma_2 \rightarrow \Pi_2$	0.75
			$6\sigma_g \rightarrow 6\pi_u$	$\Sigma_1 \rightarrow \Pi_1$	0.67
			$2\pi_g \rightarrow 9\sigma_u$	d-band $\rightarrow \Sigma_8$	-0.19

5.92	0.13	$8\sigma_g \rightarrow 8\pi_u$	$\Sigma_5 \rightarrow \Pi_5$	-0.30
		$7\sigma_u \rightarrow 7\pi_g$	$\Sigma_4 \rightarrow \Pi_4$	-0.27
		$7\sigma_g \rightarrow 7\pi_u$	$\Sigma_3 \rightarrow \Pi_3$	-0.30
		$6\sigma_u \rightarrow 6\pi_g$	$\Sigma_2 \rightarrow \Pi_2$	-0.14
		$6\sigma_g \rightarrow 6\pi_u$	$\Sigma_1 \rightarrow \Pi_1$	-0.16
		$2\pi_g \rightarrow 9\sigma_u$	d-band $\rightarrow \Sigma_8$	-0.26
		$6\sigma_g \rightarrow 8\pi_u$	$\Sigma_1 \rightarrow \Pi_5$	0.03
5.95	0.12	$8\sigma_g \rightarrow 8\pi_u$	$\Sigma_5 \rightarrow \Pi_5$	-0.27
		$7\sigma_u \rightarrow 7\pi_g$	$\Sigma_4 \rightarrow \Pi_4$	-0.25
		$7\sigma_g \rightarrow 7\pi_u$	$\Sigma_3 \rightarrow \Pi_3$	-0.12
		$6\sigma_u \rightarrow 6\pi_g$	$\Sigma_2 \rightarrow \Pi_2$	-0.27
		$6\sigma_g \rightarrow 6\pi_u$	$\Sigma_1 \rightarrow \Pi_1$	-0.15
		$2\pi_g \rightarrow 9\sigma_u$	d-band $\rightarrow \Sigma_8$	-0.28
		$6\sigma_g \rightarrow 8\pi_u$	$\Sigma_1 \rightarrow \Pi_5$	-0.03

3.2 Absorption spectra of dimers

In this section, we analyze the changes in the optical absorption spectra of the dimers compared to the spectrum of the monomer as a function of inter-particle distance. For this, we examine the evolution of the absorption spectra as the separation distance decreases from 2 nm to 0.4 nm using increments of 0.1 nm (Figure 5). When the monomers are separated by large distances from each other (i.e. above approximately 0.7 nm), the dimer spectrum are similar to the spectrum of the monomer except that the intensities of both longitudinal and transverse peaks are doubled due to the presence of two monomers. However, when the separation between the monomers is less than 0.7 nm, a new peak (called a charge transfer peak in this text, which will be verified later in this work) begins to emerge between the longitudinal and the transverse peak for all investigated systems (Ag_4, Ag_6 and Ag_{10}). This peak emerges between 4 eV and 5 eV for every system. It increases in intensity and red-shifts from its initial position as the separation between monomers further decreases. Correspondingly, the intensity of the transverse peak also decreases.

In order to study the origin of the charge transfer peak, such as whether or not it is part of transverse peak that has red shifted from the transverse peak position, we computed the spectra at additional separation distances between 0.7 nm and 0.6 nm. Spectra at some of these distances are included in Figure 5b for the Ag_6 dimer. These spectra show that the peak does not shift continuously from the transverse peak position. It appears between 4 eV and 5 eV for every system as the distance decreases; upon further decreasing the inter-particle distance, the charge-transfer peak starts to red-shift from its position and increases in intensity.

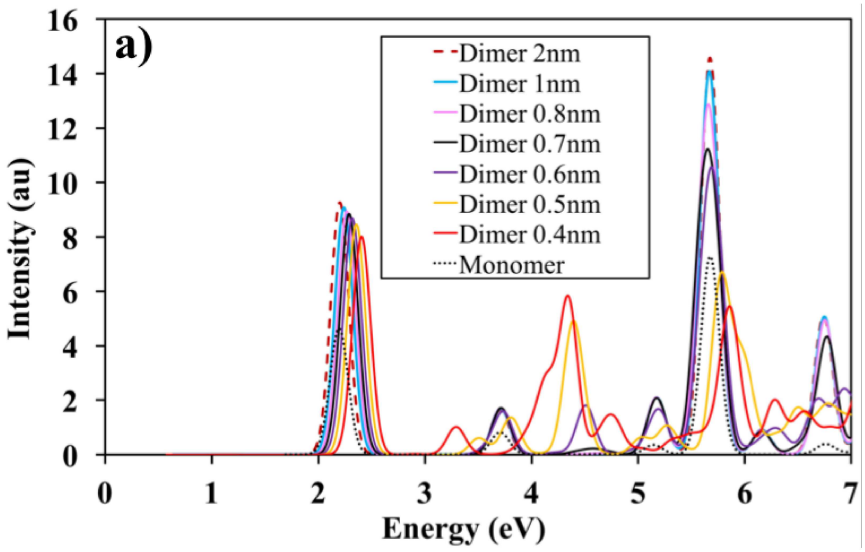
a)
Dimer 2nm
Dimer 1nm
Dimer 0.8nm
Dimer 0.7nm
Dimer 0.6nm
Dimer 0.5nm
Dimer 0.4nm
Monomer
Intensity (au)
Energy (eV)

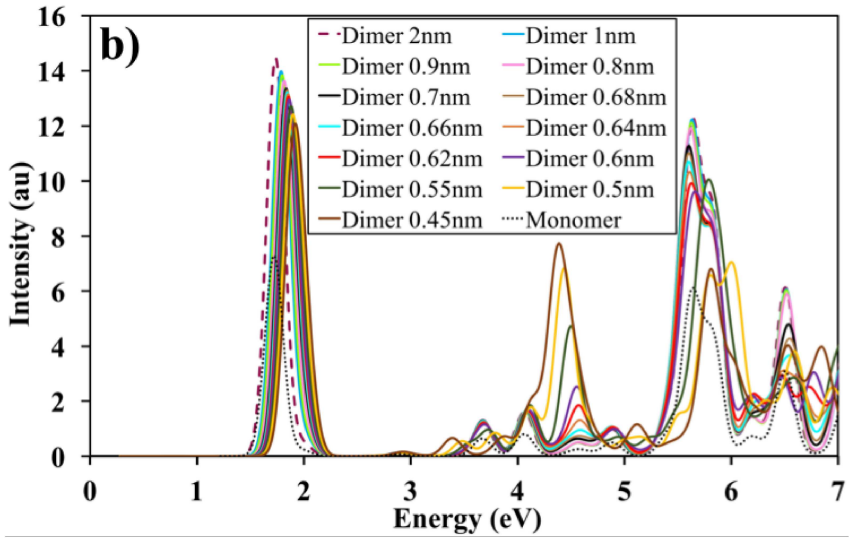
b)
Dimer 2nm
Dimer 1nm
Dimer 0.9nm
Dimer 0.8nm
Dimer 0.7nm
Dimer 0.68nm
Dimer 0.66nm
Dimer 0.64nm
Dimer 0.62nm
Dimer 0.6nm
Dimer 0.55nm
Dimer 0.5nm
Dimer 0.45nm
Monomer
Intensity (au)
Energy (eV)

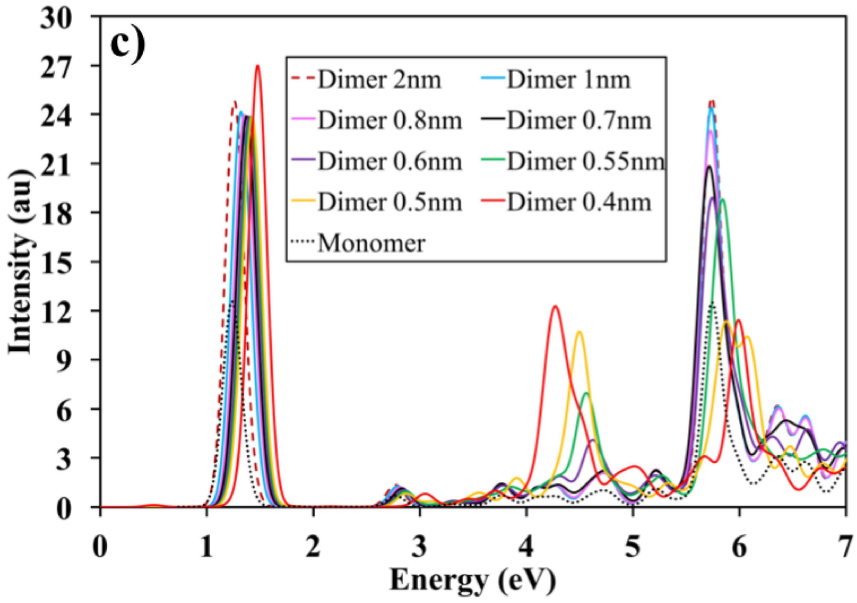
c)
Dimer 2nm
Dimer 1nm
Dimer 0.8nm
Dimer 0.7nm
Dimer 0.6nm
Dimer 0.55nm
Dimer 0.5nm
Dimer 0.4nm
Monomer
Intensity (au)
Energy (eV)

Figure 5. Absorption spectra for the dimers of a) Ag_4, b) Ag_6 and c) Ag_{10} nanowires. Spectra for only selected inter-particle distances are shown for clarity.

The longitudinal peak of the dimer blue-shifts slightly with decreasing gap distance (Figure 5). The intensity of this peak decreases as the inter-particle separation decreases. The blue-shift of longitudinal peak can be well explained using the concept of plasmon hybridization.[58] Plasmons can couple based on the dipole-dipole interaction model as shown in Figure 6. Hybridization results from coupling of plasmon modes analogous to bonding and antibonding interactions of molecular orbitals. The blue-shift of the longitudinal peak with the decrease in the gap is due to the bright mode being higher in energy which is a result of the repulsive dipole-dipole interaction between nanowires as shown in Figure 6. As the separation between monomers decreases, the interaction between the nanowires leads to a greater separation between bright and dark modes. Since the higher energy mode is the bright mode, the longitudinal peak blue-shifts on decreasing the separation between the monomers.

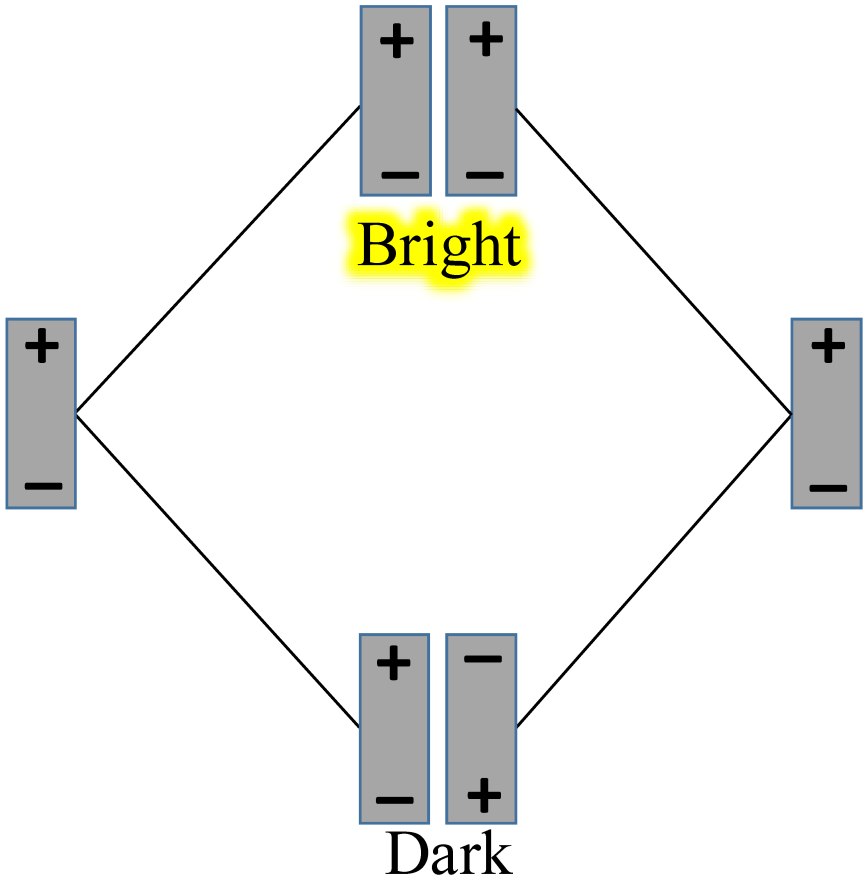

Figure 6. Longitudinal plasmon interaction that cause blue-shift in peak position in decreasing the gap between monomers

Symmetry analysis of individual peaks shows that the longitudinal peak has B_{1u} (z-polarized) symmetry while the transverse peak has both B_{2u} (y-polarized) and B_{3u} (x-polarized)

symmetry. If one examines the orbital transitions and the symmetry of the charge transfer peak, it can be seen that the charge transfer peak has only a B_{2u} symmetry contribution. The appearance of the charge transfer peak becomes more clear by studying the transverse plasmons in each nanowire monomer and the interaction between them. The inter-particle interactions between the B_{2u} and B_{3u} plasmon modes that contribute to the transverse plasmon peak are shown schematically in Figure 7. The *x*-polarized plasmon and *y*-polarized plasmon interactions yield a bright mode for the higher and lower energy levels, respectively. The charge transfer peak has B_{2u} symmetry, similar to the *y*-polarized transverse mode. Because of the geometrical considerations, the interaction between the *y*-polarized transverse modes is stronger compared to the interaction between *x*-polarized transverse modes as the gap distance decreases between monomers. As a result, the *y*-polarized plasmon peak exhibits more splitting of its energy levels which causes its bright mode to red-shift. The interaction between the *x*-polarized plasmon increases upon decreasing the separation, but it is less compared to that of the *y*-polarized plasmon. In consequence, the plasmon peak with B_{3u} symmetry shifts slightly towards the higher energy side but this shift is less compared to that of the B_{2u} plasmon peak.

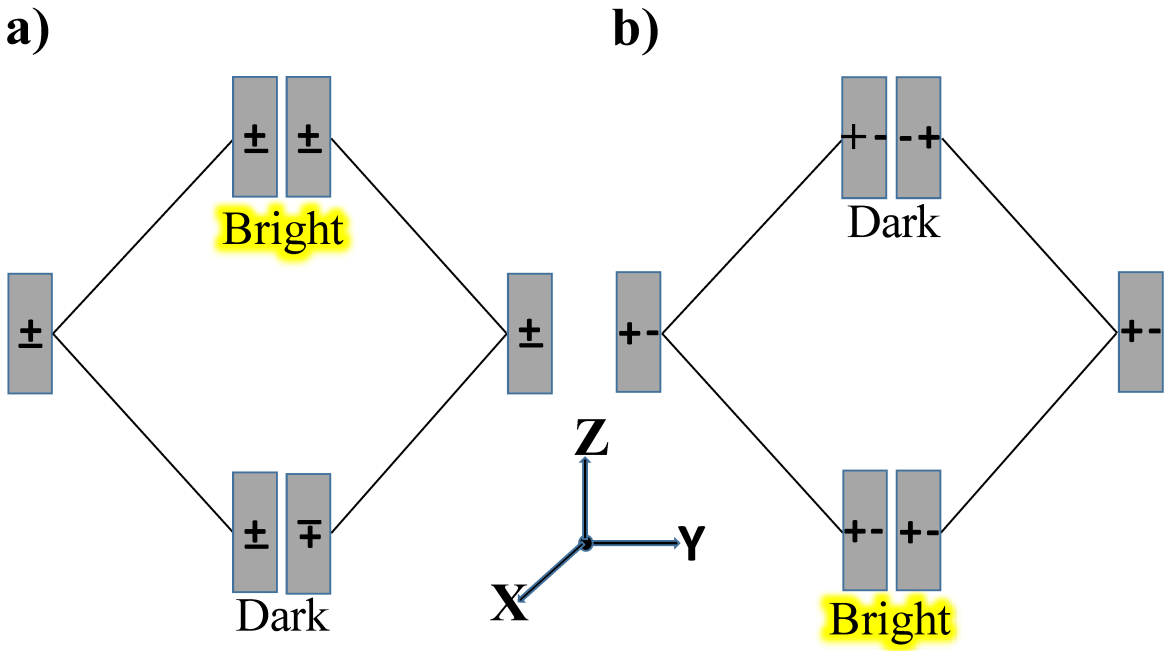

Figure 7. Transverse plasmon interaction in nanowires a) *x*-polarized, b) *y*-polarized. The long axis of the nanowires lies along the z-axis and the inter-particle axis is the y-axis.

When we look at the optical absorption spectrum for each dimer (Figure 5), the new feature in the spectrum (the charge-transfer peak) grows as the inter-particle separation is decreased. The charge transfer peak increases in intensity whereas the transverse peak decreases in intensity upon decreasing the separation between monomers. This supports the idea that this peak is related to the transverse plasmon mode, although it is not simply a red-shifted transverse peak.

To investigate further, we plotted separate absorption spectra for each of the symmetries (plasmon polarization directions) that contribute to the overall absorption spectra for the dimers of Ag_4, Ag_6 and Ag_{10} nanowires (Figures S2 and S3). The charge transfer peak has only B_{2u} symmetry which is the symmetry group of the *y*-polarized transverse mode of the plasmon (i.e. the transverse mode that is polarized along the inter-particle axis). The transverse peak around 5.7 eV does not continuously red-shift with decreasing inter-particle distance to create the charge transfer peak near 4.3 eV. Instead, the charge transfer appears when the inter-particle distance is approximately 0.7 nm, and increases in intensity dramatically and red-shifts slightly as the inter-particle distance decreases; in contrast, at separation distances below 0.7 nm, the *y*-polarized transverse mode near 5.7 eV shifts to higher energy (reversing its previous trend toward lower energy) and decreases in intensity.

We also see from Figure 5 that the intensity of the longitudinal peak becomes smaller with decreasing gap distance in all dimers. Similarly, Figure S2 and Figure S3 show that the B_{1u} peak is shifting to higher energy at smaller inter-particle distance. On looking at the spectra of Ag_{10} at the 0.4 nm inter-particle distance in Figure 5, we see that the intensity increases instead of decreasing unlike in other dimer systems and at other inter-particle separations. The cause of this can be understood by considering the peak contributions. Symmetry contribution plots for Ag_{10} (Figure S3) show that B_{2u} symmetry also contributes to the longitudinal peak at the 0.4 nm inter-particle distance for this nanowire. However in other systems, there is no other symmetry contribution to the longitudinal peak except B_{1u} at any separation. This extra B_{2u} may have increased the intensity of Ag_{10} at 0.4 nm.

Overall, in the case of larger gap distances, the quantum mechanical effects can be neglected. However, as the gap distance become less than 0.7 nm, quantum mechanical effects become important. We see that the new charge transfer peaks appear at small monomer separations which is likely caused due to the overlapping of the electron densities of the two closely placed nanoparticles (Figure 5).

3.2(a) Symmetries, transitions and orbitals for the main absorption peaks in dimers

Table 3 lists the main transitions, symmetry and orbitals for the longitudinal peak of Ag_4, Ag_6 and Ag_{10} nanowire dimers. It is clear from the table that the longitudinal peak of all nanowire dimers have $\Sigma \rightarrow \Sigma$ transitions with B_{1u} symmetry. For dimers at all separations, the longitudinal peak arises due to $\Sigma_n^* \rightarrow \Sigma_{n+1}^*$ and $\Sigma_n \rightarrow \Sigma_{n+1}$ transitions with B_{1u} symmetry. The symmetry contribution (B_{1u}) and the type of orbital transitions ($\Sigma \rightarrow \Sigma$) that corresponds to the longitudinal peak of dimers do not change with the change in inter-particle distance. So, the symmetry and transitions given in Table 3 are applicable to the dimers at all inter-particle separation. However, it should be noted that a small B_{2u} contribution does arise at 0.4 nm for the Ag_{10} dimer as seen in Figure S3.

Symmetry contributions to the transverse peak are different at large and small inter-particle distances, unlike for the longitudinal peak. Table 4 shows the transitions that contribute to the transverse peak of Ag_4 dimer at large (2 nm) and small (0.4 nm) inter-particle distance. B_{2u} and B_{3u} symmetries contribute to the transverse peak at large separation whereas at small separation, only the B_{3u} symmetry contributes to the transverse peak. Table 4 shows that the transverse peak in dimers is due to $\Sigma_n^* \rightarrow \Pi_n^*$and $\Sigma_n \rightarrow \Pi_n$ with B_{3u} symmetry as well as $\Sigma_n \rightarrow \Pi_n^*$ and $\Sigma_n^* \rightarrow \Pi_n$ transitions with B_{2u} symmetry at large inter-particle separation (2 nm). At interacting inter-particle distance (0.4 nm), only transitions with B_{3u} symmetry contribute to the transverse peak and B_{2u} symmetry transitions no longer contribute to the transverse peak. Ag_6 and Ag_{10} dimers have the

same symmetry contributions and similar transitions including some additional transitions in between the orbitals having more number of nodes. For the naming of orbitals, the Greek letter and the subscript denote the delocalized monomer orbitals involved in the dimer orbital and a "*" denotes an inter-particle antibonding nature of the monomer orbitals as shown in Figure 8. Overall, the transitions in Table 3, Table 4 and Table 5 show that the $\Sigma \rightarrow \Sigma$ transitions contribute to the longitudinal peak whereas the transverse and charge transfer peak have $\Sigma \rightarrow \Pi$ transitions. Figure 8 shows some of the orbitals that contribute to these peaks.

Table 3. Symmetry, main transitions and orbital contributions for the longitudinal peak of dimers.

Nanowire	Symmetry	Transitions (Symmetry representation)	Transitions (Delocalized orbital notation)
Ag_4	B_{1u}	$7b_{3g} \rightarrow 8b_{2u}$	$\Sigma_2^* \rightarrow \Sigma_3^*$
		$7b_{1u} \rightarrow 8a_g$	$\Sigma_2 \rightarrow \Sigma_3$
Ag_6	B_{1u}	$11b_{2u} \rightarrow 11b_{3g}$	$\Sigma_3^* \rightarrow \Sigma_4^*$
		$11a_g \rightarrow 11b_{1u}$	$\Sigma_3 \rightarrow \Sigma_4$
Ag_{10}	B_{1u}	$18b_{2u} \rightarrow 18b_{3g}$	$\Sigma_5^* \rightarrow \Sigma_6^*$
		$18a_g \rightarrow 18b_{1u}$	$\Sigma_5 \rightarrow \Sigma_6$

Table 4. Symmetry, main transitions and orbital contributions for the transverse peak of Ag_4 dimer at large and small separation.

Separation	Symmetry	Transitions (Symmetry representation)	Transitions (Delocalized orbital notation)
2 nm	B_{3u}	$7b_{1u} \rightarrow 5b_{2g}$	$\Sigma_2 \rightarrow \Pi_2$
		$7b_{3g} \rightarrow 5a_u$	$\Sigma_2^* \rightarrow \Pi_2^*$
		$7a_g \rightarrow 5b_{3u}$	$\Sigma_1 \rightarrow \Pi_1$
		$7b_{2u} \rightarrow 5b_{1g}$	$\Sigma_1^* \rightarrow \Pi_2^*$
	B_{2u}	$7b_{1u} \rightarrow 9b_{3g}$	$\Sigma_2 \rightarrow \Pi_2^*$
		$7b_{3g} \rightarrow 9b_{1u}$	$\Sigma_2^* \rightarrow \Pi_2$
		$7a_g \rightarrow 9b_{2u}$	$\Sigma_1 \rightarrow \Pi_1^*$
		$7b_{2u} \rightarrow 9a_g$	$\Sigma_1^* \rightarrow \Pi_1$
0.4 nm	B_{3u}	$7b_{1u} \rightarrow 5b_{2g}$	$\Sigma_2 \rightarrow \Pi_2$
		$7a_g \rightarrow 5b_{3u}$	$\Sigma_1 \rightarrow \Pi_1$
		$7b_{3g} \rightarrow 5a_u$	$\Sigma_2^* \rightarrow \Pi_2^*$
		$7b_{2u} \rightarrow 5b_{1g}$	$\Sigma_1^* \rightarrow \Pi_1^*$

Table 5. Symmetry, main transitions and orbital contributions for the charge transfer peak of dimers at 0.5 nm.

Nanowire	Symmetry	Transitions (Symmetry representation)	Transitions (Delocalized orbital notation)
Ag_4	B_{2u}	$7b_{3g} \rightarrow 9b_{1u}$	$\Sigma_2^* \rightarrow \Pi_2$
		$7b_{2u} \rightarrow 9a_g$	$\Sigma_2^* \rightarrow \Pi_2$

		$11b_{2u} \rightarrow 14a_g$	$\Sigma_3^* \rightarrow \Pi_3$
Ag_6	B_{2u}	$10b_{3g} \rightarrow 13b_{1u}$	$\Sigma_2^* \rightarrow \Pi_2$
		$10b_{2u} \rightarrow 13a_g$	$\Sigma_1^* \rightarrow \Pi_1$
		$18b_{2u} \rightarrow 24a_g$	$\Sigma_5^* \rightarrow \Pi_5$
		$17b_{3g} \rightarrow 22b_{1u}$	$\Sigma_4 \rightarrow \Pi_4$
Ag_{10}	B_{2u}	$17b_{2u} \rightarrow 22a_g$	$\Sigma_3^* \rightarrow \Pi_3$
		$16b_{3g} \rightarrow 20b_{1u}$	$\Sigma_2^* \rightarrow \Pi_2$
		$16b_{2u} \rightarrow 21a_g$	$\Sigma_1^* \rightarrow \Pi_1$

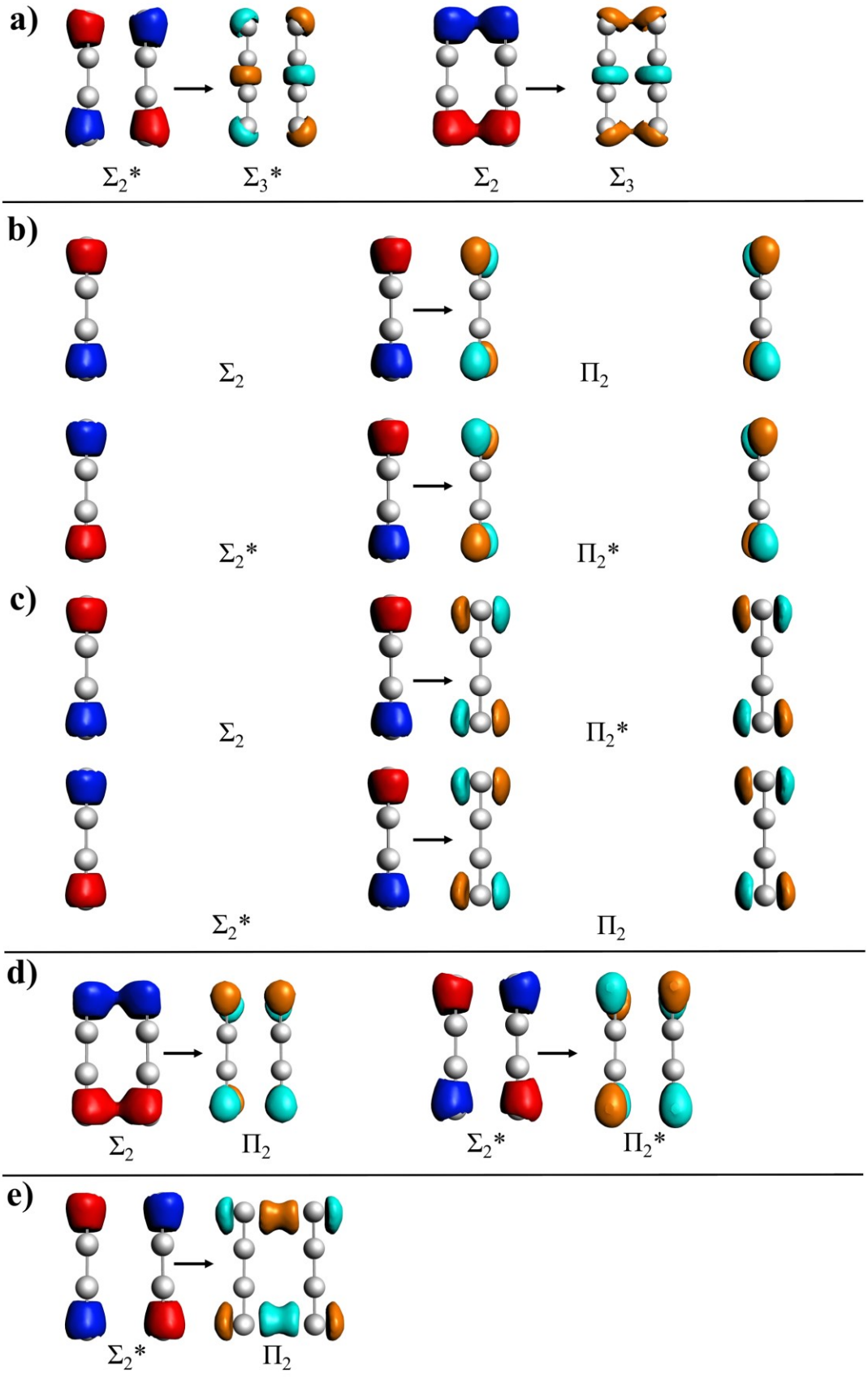
a)
Σ_2*
Σ_3*
Σ_2
Σ_3
b)
Σ_2
Π_2
Σ_2*
Π_2*
c)
Σ_2
Π_2*
Σ_2*
Π_2
d)
Σ_2
Π_2
Σ_2*
Π_2*
e)
Σ_2*
Π_2

Figure 8. Examples of occupied-to-virtual orbital transitions contributing to the (a) longitudinal peak of Ag_4 dimer as shown in Table 3, (b) transverse peak of Ag_4 dimer at 2 nm separation and with B_{3u} symmetry as shown in Table 4, (c) transverse peak of Ag_4 dimer at 2 nm separation and with B_{2u} symmetry as shown in Table 4, (d) transverse peak of Ag_4 dimer at 0.4 nm separation as shown in Table 4, (e) charge transfer peak of the Ag_4 dimer at 0.5 nm as shown in Table 5 drawn with a contour value of 0.03.

3.2(b) Transition electron densities

In order to understand more about the types of transitions that make up the different peaks in the absorption spectra, we studied the transition densities for the strongest excited state (i.e. the excited state with the highest oscillator strength) corresponding to each plasmon peak (Figure 9). These transition densities are shown for inter-particle distances of 2 nm (large separation between the monomers) and 0.5 nm (small separation between the monomers) for the Ag_4 nanowire dimer. Transition densities were similarly studied for other separations as well (not shown). The transition densities of other close-lying excitations with smaller oscillator strengths are similar to those of the strong excitations as shown in the Supporting Information (Figure S4).

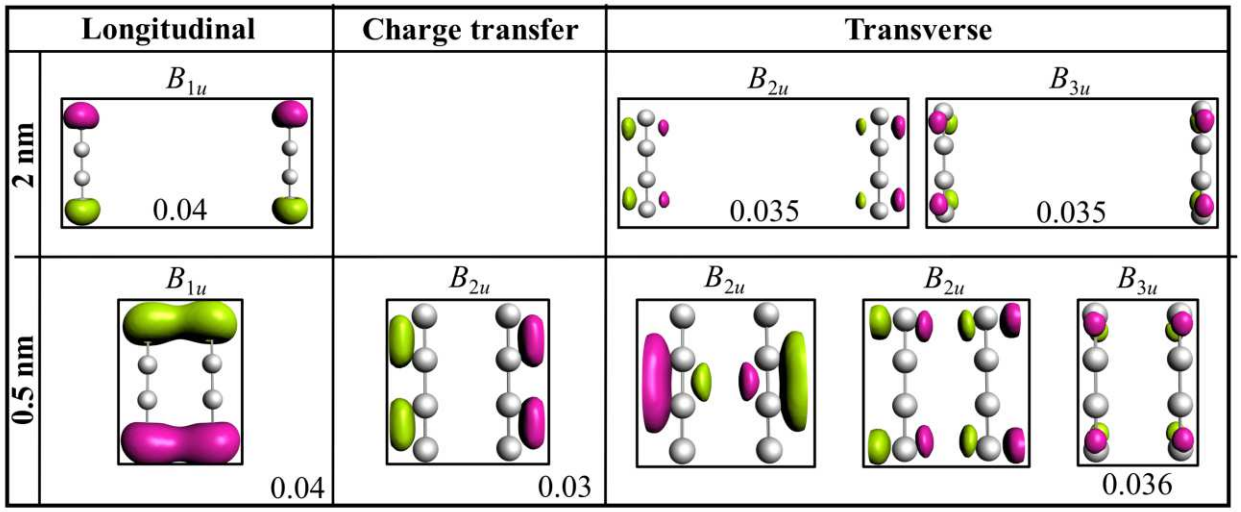

Figure 9. Transition electron densities for the strongest peaks of Ag_4 dimer at the iso-value of 0.02 unless stated in inset.

In Figure 9, transition electron densities for the longitudinal peak at both large and small separation show longitudinal character (i.e. the movement of electron density along the long axis). Similarly, the transition electron densities for the transverse peaks at all separations show transverse character where the movement of electron density is perpendicular to the long axis. The charge transfer peak does not appear when the inter-particle distance is large (e.g. 2 nm), whereas it appears for small inter-particle distances (e.g. 0.5 nm). The transition densities demonstrate that this peak has charge transfer character because the movement of electron density occurs from one wire to the other. Transition electron densities for the middle peak of Ag_6 and Ag_{10} are given in the supporting information (Figure S5) which show similar charge transfer character.

Overall, from 2 nm until 0.7 nm, there is very little coupling between the nanowires. After 0.7 nm, the coupling between the nanowires favors the tunneling of electrons between the two monomers. In consequence, quantum mechanical effects are especially necessary to include at small separation distances.

Because calculations with pure GGA functional are known to overestimate charge transfer,[111] we also performed calculations using the time-dependent Hartree-Fock (TDHF) approximation to examine whether any charge transfer artifacts arise due to the use of the GGA functional (Figure 10). Although the longitudinal and transverse peak positions obtained with TDHF are somewhat shifted compared to the peak positions obtained with the GGA functional, both levels of theory agree on the formation of a charge transfer peak with B_{2u} symmetry that occurs between 4 eV and 5 eV and has charge transfer character in the transition electron density (Figure 10). A picture of the spectra obtained with TDHF calculation at different monomer separations along with their transition density plots are shown in Figure S6. One noticeable difference between the TDDFT calculations (with a pure GGA functional) and the TDHF calculations is that the charge transfer peak shifts gradually during the TDHF calculations, unlike in the TDDFT calculations; this is likely due to differences in the interaction term between the excited determinants as previously observed in TDHF and TDDFT calculations on nanowires arranged in an end-to-end fashion.[88] This suggests that the sudden appearance of the charge-transfer peak in calculations using a pure GGA functional may be an artifact, although the existence of the charge-transfer peak is not.

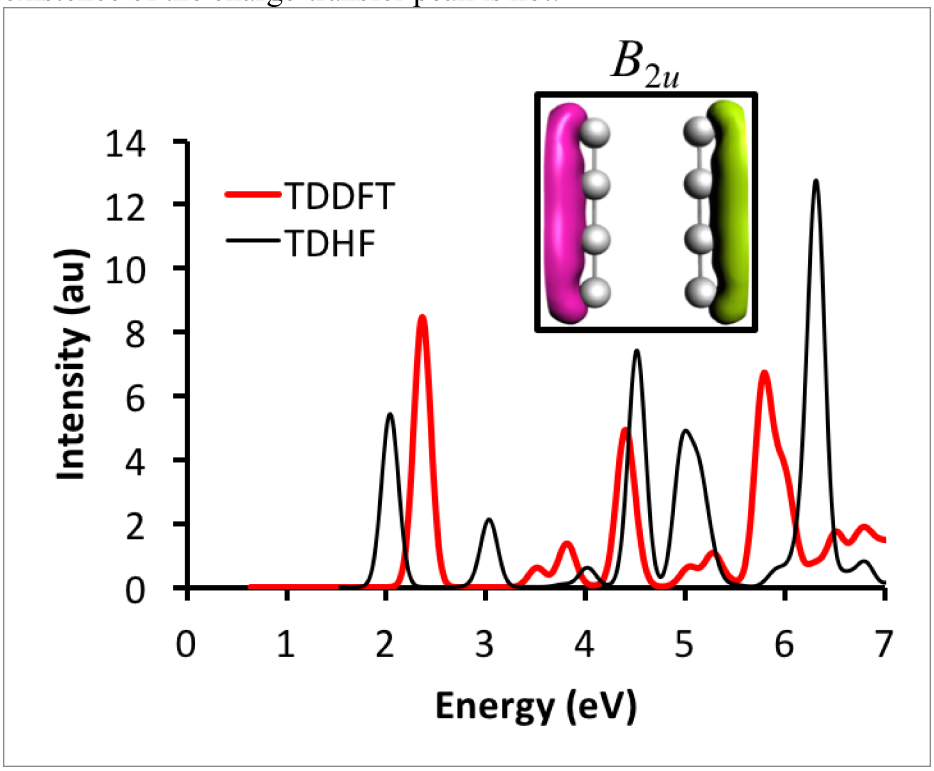

Figure 10. Optical absorption spectra showing the main peaks computed with TDDFT (red plot) and TDHF (black plot). The inset shows the TDHF transition electron density (iso-value = 0.03) for the charge transfer peak between 4 eV and 5 eV with B_{2u} symmetry.

3.3 Absorption spectra of trimers

Absorption spectra are also obtained for trimers of Ag_n ($n = 4, 6, 10$) in the dolmen structure with C_{2v} symmetry. Spectra for the Ag_4 trimer at inter-particle distances of 2 nm to 0.4 nm are shown in Figure 11. Spectra for Ag_6 and Ag_{10} trimers at different inter-particle separations have similar trends (Figure S7). Throughout this section, the Ag_6 and Ag_{10} trimers yield the same results as Ag_4 and are not discussed in detail.

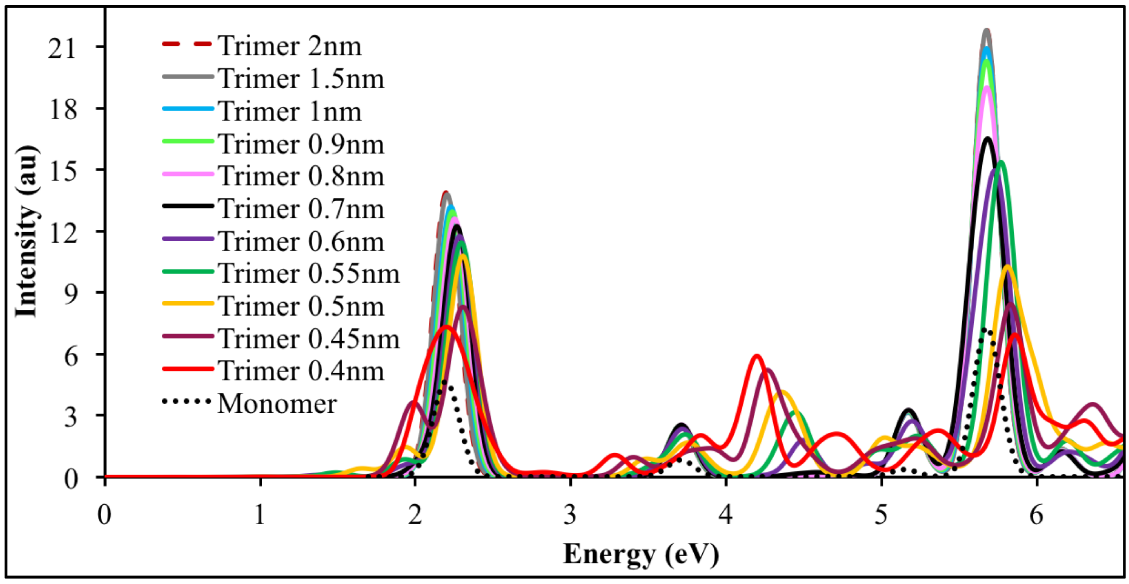

Figure 11. Absorption spectra for Ag_4 trimer

A blue-shift of the longitudinal peak is apparent in the trimer similar to the dimer, but additional shoulder peaks are also seen on the lower energy side when the monomer separation is 0.6 nm or less. The intensity of the shoulder peak increases upon decreasing the separation between the monomers. At 0.45 nm, the peak no longer blue-shifts and instead its energy remains constant. At 0.4 nm, the shoulder peak is not noticeable due to the employed smoothing, but it is still present. The intensity of the longitudinal peak decreases more for the trimers when compared to the case in the dimers for decreasing gap distance.

For the dimer structure, both nanowires lie on the z-axis, so there is interaction only between the two *z*-polarized plasmons for the longitudinal peak of the dimer. In the trimer, one difference compared to the longitudinal peak of the dimer is that there are many possible interactions between the different plasmon modes in the three nanowires (Figure S8). Because the parallel dimer is aligned on the z-axis, the longitudinal peak is the *z*-polarized plasmon. However, because the long axis of the capping monomer lies on the y-axis in the trimer, the *y*-polarized plasmon also contributes to the longitudinal peak as also observed in the absorption spectrum. At small separation distances, there are significant interactions between the monomer plasmons that give different symmetries for the longitudinal peak. These interactions give rise to other unique features in the trimer spectra compared to the dimer spectra. For the C_{2v} trimer, two symmetries contribute to the longitudinal peak in the trimer: A_1 (*z*-polarized) from the parallel dimer and B_2 (*y*-polarized) from the capping nanowire. The transition electron densities of the most important excitations that that contribute to the longitudinal peak of the Ag_4 trimer obtained at different inter-particle separations are given in Figure S9. Absorption spectra for the individual symmetry

contributions of the Ag_4 trimer are also plotted which clearly show the symmetry contributions to the different peaks (Figure S10).

Similarly, the transverse plasmons have different polarization directions. Unlike in the dimer transverse peak, a *z*-polarized excitation also contributes to the transverse peak of the trimer because it is the transverse plasmon peak of the capping nanowire (Figure 12a). The transverse plasmon oscillations in capping nanowires interact with the bright and dark modes obtained from the transverse oscillations in dimer nanowires. An interaction picture of the bright modes from Figure 7 with different possible plasmon oscillations of the capping nanowire is illustrated in Figure 12. The *y*-polarized transverse dimer plasmon interacts with the *y*-polarized plasmon in the capping nanowire; similarly, the *x*-polarized plasmon from the dimer interacts with the *x*-polarized plasmon in the capping nanowire. Overall, the transverse peak in trimer has A_1 (from *z*-polarized transverse plasmon of capping monomer as shown in Figure 12), B_1 (from *x*-polarized plasmon contribution of both dimer and capping monomer) and B_2 (from *y*-polarized transverse plasmon in dimers and capping monomer) symmetry contributions.

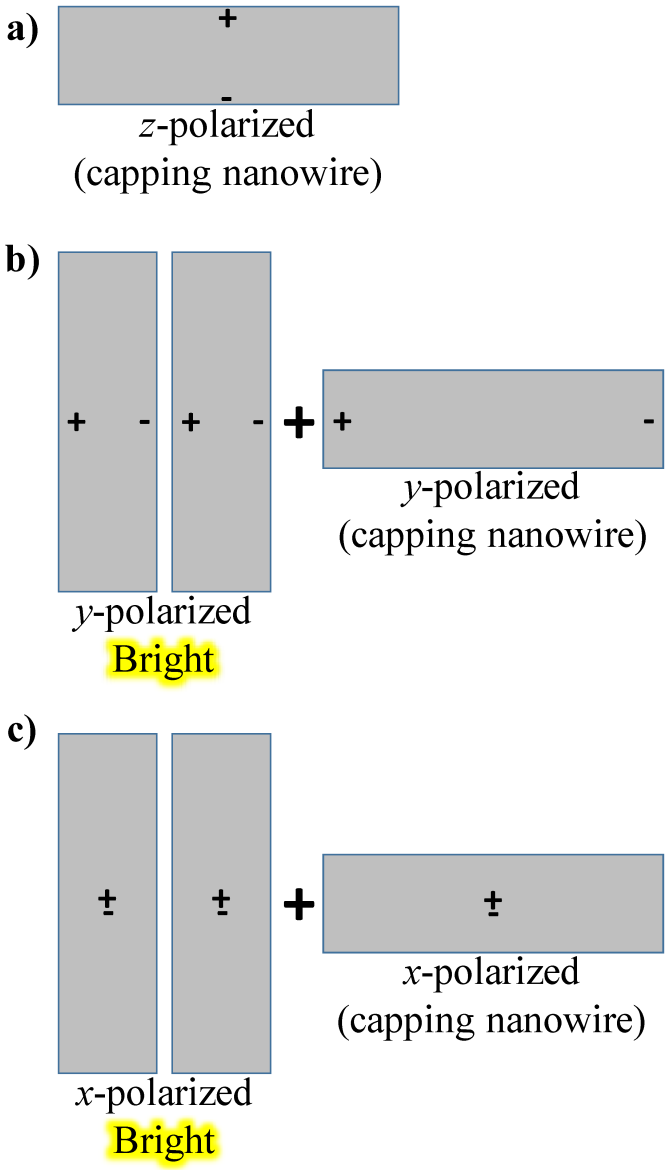

Figure 12. a) The *z*-polarized transverse plasmon in the capping nanowire which also contributes to the transverse absorption peak in the trimer system. Interaction of bright b) *y*-polarized and c) *x*-polarized transverse dimer plasmons shown in Figure 7 with *y*- and *x*- plasmon excitations from the capping nanowire, respectively.

Similar to the charge transfer peak in the dimer, the charge transfer peak in the trimer appears for monomer gaps of 0.6 nm or less and is *y*-polarized (B_2 symmetry). Upon further decreasing the inter-particle separation, the charge transfer peak red-shifts and increases in intensity while the transverse peak slightly blue-shifts and decreases in intensity, similar to the dimer spectra. It should be noted that the capping monomer plasmon has an insignificant contribution to the charge transfer peak compared to the dimer subsystem.

3.3(a) Symmetry, transitions and orbitals for the main peaks in trimers

Table 6. Symmetry, main transitions and orbital contributions for the longitudinal peak of Ag_4 trimer at large and small inter-particle separation.

Separation	Symmetry	Transitions (Symmetry representation)	Transitions (Delocalized orbital notation)
2 nm	B_2	$20b_2 \rightarrow 22a_1$	${}^{cap}\Sigma_2 \rightarrow {}^{cap}\Sigma_3$
	A_1	$21b_2 \rightarrow 22b_2$	${}^{dimer}\Sigma_2{*} \rightarrow {}^{dimer}\Sigma_3{*}$
		$21a_1 \rightarrow 23a_1$	${}^{dimer}\Sigma_2 \rightarrow {}^{dimer}\Sigma_3$
0.4 nm	B_2	$19b_2 \rightarrow 22a_1$	${}^{cap}\Sigma_2 \rightarrow {}^{cap}\Sigma_3$
	A_1	$21a_1 \rightarrow 23a_1$	${}^{dimer}\Sigma_2 \rightarrow {}^{dimer}\Sigma_3$ *and* ${}^{cap}\Sigma_1$
		$21b_2 \rightarrow 22b_2$	${}^{dimer}\Sigma_2{*} \rightarrow {}^{dimer}\Sigma_3{*}$

From Table 6, at large separations the transitions do not mix; they occur from cap to cap or from dimer to dimer. However, at small inter-particle separation (e.g. 0.4 nm), there is interaction between the capped monomer and the dimer subsystem. This kind of interaction is observed for other investigated systems Ag_6 and Ag_{10}: the interaction between the cap and the dimer part is seen only at small separation distances and is not observed at all at large separations. Thus, the capped monomer does not interact with the dimer as strongly as the two monomers in dimers interact although they are at the same separation distance.

3.3(b) Transition electron densities

Transition electron densities for the main peaks of the Ag_4 trimer are shown in Figure 13. The longitudinal peak arises from plasmon oscillation along the long axis of the parallel nanowire dimer (*z*-polarized plasmon) and in the long axis of the capping nanowire (*y*-polarized plasmon). Interaction between the dimer and the capping monomer appears at the smaller inter-particle distance of 0.5 nm but not at the larger separation. Similarly, the transition electron densities for the transverse peak of the trimer show *x*-, *y*-, and *z*- polarized plasmon contributions. The peak obtained in between 4 eV and 5 eV in the trimer has charge transfer character similar to the charge transfer peak in the dimer. Other systems (Ag_6 and Ag_{10}) have similar transition electron densities as the Ag_4 trimer system. We also performed TDHF calculations with the trimer which similarly yielded a new feature between 4 eV and 5 eV having charge transfer character. Thus, both the dimer and the dolmen trimer exhibit a new charge transfer peak for small inter-particle separations. The unique feature of the dolmen trimer compared to the dimer is the appearance of a new shoulder peak on the lower energy side of longitudinal peak. The TDDFT and TDHF transition electron densities for that peak are shown in Figure 14. We can see that TDDFT predicts that both the A_1 and B_2 symmetry contribute to this peak whereas TDHF only predicts a B_2 symmetry contribution. The transition densities with A_1 symmetry from TDDFT show charge transfer between the parallel dimer and capping monomer. However, the transition density plots with B_2 symmetry obtained from both TDDFT and TDHF do not show charge transfer character. Because charge transfer character of the longitudinal peak with A_1 symmetry is not obtained with TDHF, TDDFT appears to overestimate the charge transfer for this peak.

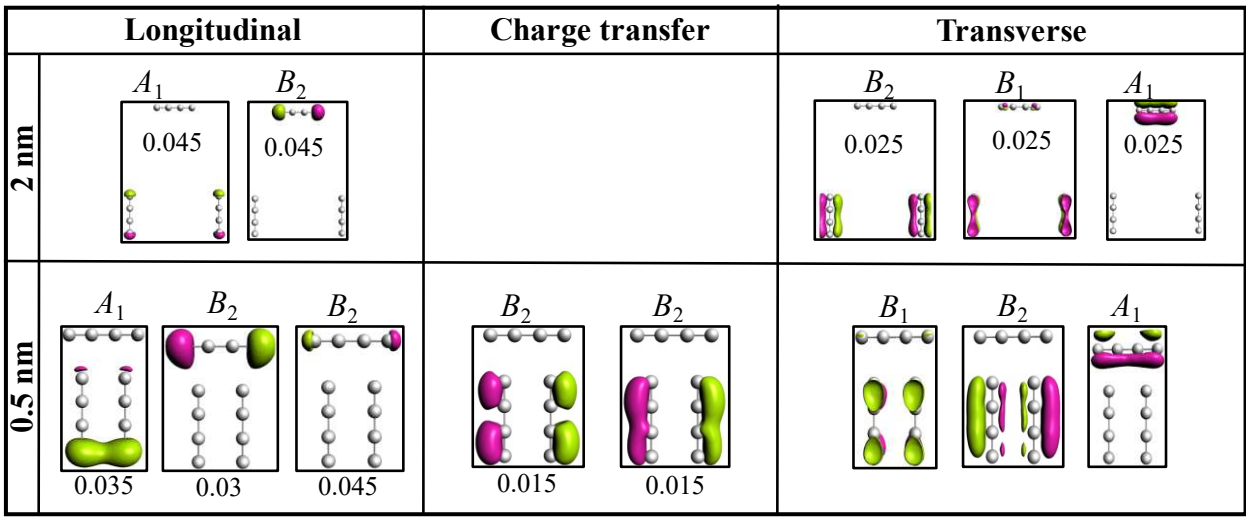

Figure 13. Transition electron densities for major peaks of Ag_4 trimer at 2 nm and 0.5 nm inter-particle distance obtained at iso-value of 0.02 unless stated.

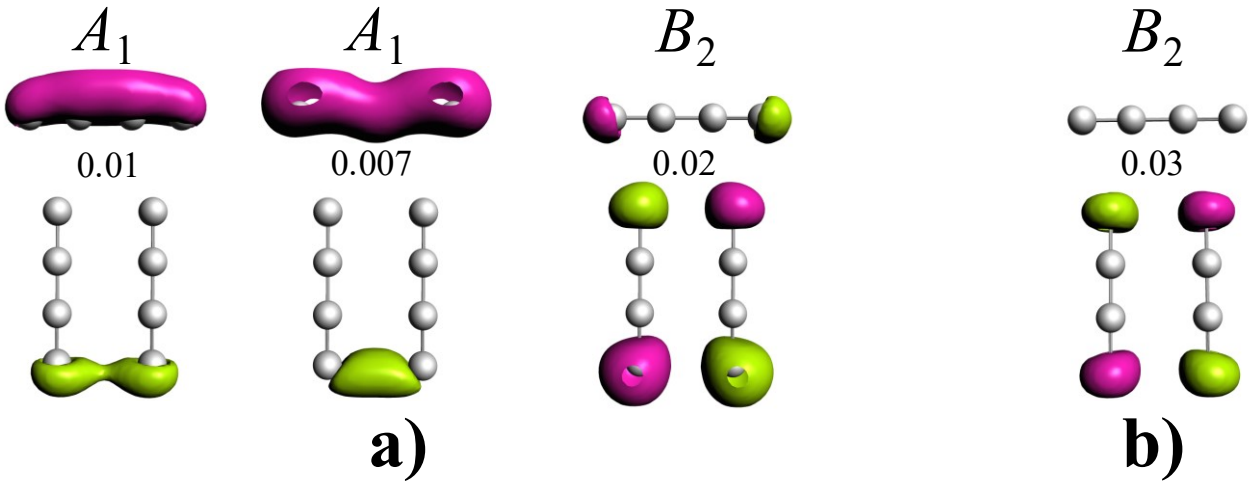

Figure 14. Transition electron density plots for the shoulder on the lower energy side of the longitudinal peak of the Ag_4 trimer at 0.5 nm interparticle distance obtained with an iso-value of 0.005 (a) from TDDFT (b) from TDHF.

4. CONCLUSION

In nanowire monomers, the longitudinal peak (Σ symmetry) is due to $\Sigma \rightarrow \Sigma$ transitions and the transverse peak (Π symmetry) arises due to $\Sigma \rightarrow \Pi$ transitions. The longitudinal peak red-shifts upon increasing the chain length. For dimers at all separations, the longitudinal peak arises due to $\Sigma_n^* \rightarrow \Sigma_{n+1}^*$ and $\Sigma_n \rightarrow \Sigma_{n+1}$ transitions with B_{1u} symmetry. The transverse peak in dimers is due to $\Sigma_n^* \rightarrow \Pi_n^*$ and $\Sigma_n \rightarrow \Pi_n$ transitions having B_{3u} symmetry and $\Sigma_n \rightarrow \Pi_n^*$ and $\Sigma_n^* \rightarrow \Pi_n$ transitions having B_{2u} symmetry at large separation; at closer interparticle distances, only B_{3u} contributes. For trimers, the longitudinal peak has contributions from B_2 and A_1 symmetry at all separation distances. At large inter-particle distances, the transitions are ${}^{cap}\Sigma_n \rightarrow {}^{cap}\Sigma_{n+1}$ with B_2 symmetry. The longitudinal peak also has ${}^{dimer}\Sigma_n^* \rightarrow {}^{dimer}\Sigma_{n+1}^*$ and ${}^{dimer}\Sigma_n \rightarrow {}^{dimer}\Sigma_{n+1}$ transitions with A_1 symmetry when the separation is large between the monomers. Thus, the transitions occur

within the same subsystem at large separation distances. When the separation between the monomers is small, transitions between the capping monomer and dimer subsystem also occur as shown in Table 6 for an interparticle distance of 0.4 nm. The transverse peak arises from B_2, B_1 and A_1 transitions at large separation distances, but only arises from B_1 and A_1 at small separations.

Overall, we used the plasmon hybridization model and electron transition densities to analyze different features in the absorption spectra of parallel dimers and dolmen trimers of linear nanowires. Plasmon resonances of composite systems are found to arise from hybridized modes of individual nanoparticle plasmons which can be helpful to tune the optical properties. The plasmon hybridization model explains the shift of plasmon peaks for different inter-particle separations. We studied the possible bright and dark modes that can arise upon interaction of nanowire monomers at different separation distances. We found that the strong coupling between the nanowires and the tunneling of electrons at short inter-particle distances in nanowire dimers and trimers favors the creation of a new charge transfer peak. At interacting inter-particle distances, the charge transfer peak originates from $\Sigma_n^* \rightarrow \Pi_n$ transitions with B_{2u} and B_2 symmetry for the dimer and trimer respectively. Time-dependent Hartree-Fock calculations confirmed the presence of the charge transfer peak in Ag_4.

We hope this study will generate new avenues in the study of plasmonics and will initiate additional research on the nature of plasmonic peaks that arise at small inter-particle distances. This study may offer a way to advance rational engineering of the desired optical response to improve light harvesting and sensing properties, thus leading to selective control of charge localization and transport.

5. SUPPORTING INFORMATION

The Supporting Information is available free of charge at

- Ag_6 monomer spectrum at small FWHM; absorption spectra for Ag_4, Ag_6 and Ag_{10} dimers and trimers at different inter-particle separations and for different state symmetries; transition densities pictures; plasmon interaction diagram; monomer coordinates.

6. ACKNOWLEDGEMENT

This material is based on work supported by the Air Force Office of Scientific Research under Grant FA9550-15-0114. The computing for this project was performed on the Beocat Research Cluster at Kansas State University, which is funded in part by NSF Grants CHE-1726332, CNS-1006860, EPS-1006860, and EPS-0919443.

REFERENCE

1. Kelly, K. L.; Coronado, E.; Zhao, L. L.; Schatz, G. C. The Optical Properties of Metal Nanoparticles: The Influence of Size, Shape, and Dielectric Environment. *J. Phys. Chem. B* **2003,** *107*, 668-677.

2. Aroca, R.; Price, B. A New Surface for Surface-Enhanced Infrared Spectroscopy: Tin Island Films. *J. Phys. Chem. B* **1997,** *101*, 6537-6540.

3. Wang, Z.; Pan, S.; Krauss, T. D.; Du, H.; Rothberg, L. J. The Structural Basis for Giant Enhancement Enabling Single-Molecule Raman Scattering. *Proc. Natl. Acad. Sci. U.S.A* **2003,** *100*, 8638-8643.

4. Nie, S.; Emory, S. R. Probing Single Molecules and Single Nanoparticles by Surface-Enhanced Raman Scattering. *Science* **1997,** *275*, 1102-1106.
5. Michaels, A. M.; Nirmal, M.; Brus, L. E. Surface Enhanced Raman Spectroscopy of Individual Rhodamine 6G Molecules on Large Ag Nanocrystals. *J. Am. Chem. Soc.* **1999,** *121*, 9932-9939.
6. Oldenburg, S. J.; Averitt, R. D.; Westcott, S. L.; Halas, N. J. Nanoengineering of Optical Resonances. *Chem. Phys. Lett.* **1998,** *288*, 243-247.
7. Graf, C.; van Blaaderen, A. Metallodielectric Colloidal Core−Shell Particles for Photonic Applications. *Langmuir* **2002,** *18*, 524-534.
8. Nicewarner-Peña, S. R.; Freeman, R. G.; Reiss, B. D.; He, L.; Peña, D. J.; Walton, I. D.; Cromer, R.; Keating, C. D.; Natan, M. J. Submicrometer Metallic Barcodes. *Science* **2001,** *294*, 137-141.
9. Jana, N. R.; Gearheart, L.; Murphy, C. J. Wet Chemical Synthesis of High Aspect Ratio Cylindrical Gold Nanorods. *J. Phys. Chem. B* **2001,** *105*, 4065-4067.
10. Maillard, M.; Giorgio, S.; Pileni, M.-P. Tuning the Size of Silver Nanodisks with Similar Aspect Ratios: Synthesis and Optical Properties. *J. Phys. Chem. B* **2003,** *107*, 2466-2470.
11. Sun, Y.; Xia, Y. Shape-Controlled Synthesis of Gold and Silver Nanoparticles. *Science* **2002,** *298*, 2176-2179.
12. Szymańska-Chargot, M.; Gruszecka, A.; Smolira, A.; Bederski, K.; Głuch, K.; Cytawa, J.; Michalak, L. Formation of Nanoparticles and Nanorods Via UV Irradiation of $AgNO_3$ Solutions. *J. Alloys Compd.* **2009,** *486*, 66-69.
13. Kasture, M.; Sastry, M.; Prasad, B. L. V. Halide Ion Controlled Shape Dependent Gold Nanoparticle Synthesis with Tryptophan as Reducing Agent: Enhanced Fluorescent Properties and White Light Emission. *Chem. Phys. Lett.* **2010,** *484*, 271-275.
14. Aizpurua, J.; Hanarp, P.; Sutherland, D. S.; Käll, M.; Bryant, G. W.; García de Abajo, F. J. Optical Properties of Gold Nanorings. *Phys. Rev. Lett.* **2003,** *90*, 057401.
15. Al-Sherbini, E.-S. A. M. UV–Visible Light Reshaping of Gold Nanorods. *Mater. Chem. Phys.* **2010,** *121*, 349-353.
16. Ni, W.; Ambjörnsson, T.; Apell, S. P.; Chen, H.; Wang, J. Observing Plasmonic−Molecular Resonance Coupling on Single Gold Nanorods. *Nano Lett.* **2010,** *10*, 77-84.
17. Schmucker, A. L.; Harris, N.; Banholzer, M. J.; Blaber, M. G.; Osberg, K. D.; Schatz, G. C.; Mirkin, C. A. Correlating Nanorod Structure with Experimentally Measured and Theoretically Predicted Surface Plasmon Resonance. *ACS Nano* **2010,** *4*, 5453-5463.
18. Olofsson, L.; Rindzevicius, T.; Pfeiffer, I.; Käll, M.; Höök, F. Surface-Based Gold-Nanoparticle Sensor for Specific and Quantitative DNA Hybridization Detection. *Langmuir* **2003,** *19*, 10414-10419.
19. McFarland, A. D.; Van Duyne, R. P. Single Silver Nanoparticles as Real-Time Optical Sensors with Zeptomole Sensitivity. *Nano Lett.* **2003,** *3*, 1057-1062.
20. Noginov, M. A.; Zhu, G.; Belgrave, A. M.; Bakker, R.; Shalaev, V. M.; Narimanov, E. E.; Stout, S.; Herz, E.; Suteewong, T.; Wiesner, U. Demonstration of a Spaser-Based Nanolaser. *Nature* **2009,** *460*, 1110-1112.
21. Xu, H.; Bjerneld, E. J.; Käll, M.; Börjesson, L. Spectroscopy of Single Hemoglobin Molecules by Surface Enhanced Raman Scattering. *Phys. Rev. Lett.* **1999,** *83*, 4357-4360.

22. Nie, S.; Emory, S. R. Probing Single Molecules and Single Nanoparticles by Surface-Enhanced Raman Scattering. *Science* **1997,** *275*, 1102-1106.
23. Quinten, M.; Leitner, A.; Krenn, J. R.; Aussenegg, F. R. Electromagnetic Energy Transport Via Linear Chains of Silver Nanoparticles. *Opt. Lett.* **1998,** *23*, 1331-1333.
24. Maier, S. A.; Kik, P. G.; Atwater, H. A.; Meltzer, S.; Harel, E.; Koel, B. E.; Requicha, A. A. G. Local Detection of Electromagnetic Energy Transport Below the Diffraction Limit in Metal Nanoparticle Plasmon Waveguides. *Nat. Mater.* **2003,** *2*, 229-232.
25. Brongersma, M. L.; Hartman, J. W.; Atwater, H. A. Electromagnetic Energy Transfer and Switching in Nanoparticle Chain Arrays Below the Diffraction Limit. *Phys. Rev. B* **2000,** *62*, R16356-R16359.
26. Vasilantonakis, N.; Nasir, M. E.; Dickson, W.; Wurtz, G. A.; Zayats, A. V. Bulk Plasmon-Polaritons in Hyperbolic Nanorod Metamaterial Waveguides. *Laser Photonics Rev.* **2015,** *9*, 345-353.
27. Gotschy, W.; Vonmetz, K.; Leitner, A.; Aussenegg, F. R. Thin Films by Regular Patterns of Metal Nanoparticles: Tailoring the Optical Properties by Nanodesign. *Appl. Phys. B* **1996,** *63*, 381-384.
28. Haynes, C. L.; McFarland, A. D.; Zhao, L.; Van Duyne, R. P.; Schatz, G. C.; Gunnarsson, L.; Prikulis, J.; Kasemo, B.; Käll, M. Nanoparticle Optics: The Importance of Radiative Dipole Coupling in Two-Dimensional Nanoparticle Arrays. *J. Phys. Chem. B* **2003,** *107*, 7337-7342.
29. Lamprecht, B.; Schider, G.; Lechner, R. T.; Ditlbacher, H.; Krenn, J. R.; Leitner, A.; Aussenegg, F. R. Metal Nanoparticle Gratings: Influence of Dipolar Particle Interaction on the Plasmon Resonance. *Phys. Rev. Lett.* **2000,** *84*, 4721-4724.
30. Kahl, M.; Voges, E. Analysis of Plasmon Resonance and Surface-Enhanced Raman Scattering on Periodic Silver Structures. *Phys. Rev. B* **2000,** *61*, 14078-14088.
31. Félidj, N.; Aubard, J.; Lévi, G.; Krenn, J. R.; Salerno, M.; Schider, G.; Lamprecht, B.; Leitner, A.; Aussenegg, F. R. Controlling the Optical Response of Regular Arrays of Gold Particles for Surface-Enhanced Raman Scattering. *Phys. Rev. B* **2002,** *65*, 075419.
32. Billot, L.; Lamy de la Chapelle, M.; Grimault, A. S.; Vial, A.; Barchiesi, D.; Bijeon, J. L.; Adam, P. M.; Royer, P. Surface Enhanced Raman Scattering on Gold Nanowire Arrays: Evidence of Strong Multipolar Surface Plasmon Resonance Enhancement. *Chem. Phys. Lett.* **2006,** *422*, 303-307.
33. Laurent, G.; Félidj, N.; Aubard, J.; Lévi, G.; Krenn, J. R.; Hohenau, A.; Schider, G.; Leitner, A.; Aussenegg, F. R. Surface Enhanced Raman Scattering Arising from Multipolar Plasmon Excitation. *J. Chem. Phys.* **2004,** *122*, 011102.
34. Félidj, N.; Aubard, J.; Lévi, G.; Krenn, J. R.; Hohenau, A.; Schider, G.; Leitner, A.; Aussenegg, F. R. Optimized Surface-Enhanced Raman Scattering on Gold Nanoparticle Arrays. *Appl. Phys. Lett.* **2003,** *82*, 3095-3097.
35. Biswas, S.; Duan, J.; Nepal, D.; Pachter, R.; Vaia, R. Plasmonic Resonances in Self-Assembled Reduced Symmetry Gold Nanorod Structures. *Nano Lett.* **2013,** *13*, 2220-2225.
36. Verellen, N.; Sonnefraud, Y.; Sobhani, H.; Hao, F.; Moshchalkov, V. V.; Dorpe, P. V.; Nordlander, P.; Maier, S. A. Fano Resonances in Individual Coherent Plasmonic Nanocavities. *Nano Lett.* **2009,** *9*, 1663-1667.
37. Zhang, S.; Genov, D. A.; Wang, Y.; Liu, M.; Zhang, X. Plasmon-Induced Transparency in Metamaterials. *Phys. Rev. Lett.* **2008,** *101*, 047401.

38. Halpin, A.; Mennes, C.; Bhattacharya, A.; Gómez Rivas, J. Visualizing near-Field Coupling in Terahertz Dolmens. *Appl. Phys. Lett.* **2017,** *110*, 101105.
39. Vincenot, J.; Aikens, C. M. Quantum Mechanical Examination of Optical Absorption Spectra of Silver Nanorod Dimers. In *Advances in the Theory of Atomic and Molecular Systems: Dynamics, Spectroscopy, Clusters, and Nanostructures*, Piecuch, P.; Maruani, J.; Delgado-Barrio, G.; Wilson, S., Eds. Springer Netherlands: Dordrecht, 2009; Vol. 20, pp 253-264.
40. Wang, W.; Zheng, L.; Xiong, L.; Qi, J.; Li, B. High Q-Factor Multiple Fano Resonances for High-Sensitivity Sensing in All-Dielectric Metamaterials. *OSA Continuum* **2019,** *2*, 2818-2825.
41. Wang, X.; Yao, L.; Chen, X.; Dai, H.; Wang, M.; Zhang, L.; Ni, Y.; Xiao, L.; Han, J.-B. Gap-Induced Giant Third-Order Optical Nonlinearity and Long Electron Relaxation Time in Random-Distributed Gold Nanorod Arrays. *ACS Appl. Mater. Interfaces* **2019,** *11*, 32469-32474.
42. Mercadal, P. A.; Encina, E. R.; Coronado, E. A. Colloidal Sers Substrate for the Ultrasensitive Detection of Biotinylated Antibodies Based on Near-Field Gradient within the Gap of Au Nanoparticle Dimers. *J. Phys. Chem. C* **2019,** *123*, 23577-23585.
43. Pachidis, P.; Cote, B. M.; Ferry, V. E. Tuning the Polarization and Directionality of Photoluminescence of Achiral Quantum Dot Films with Chiral Nanorod Dimer Arrays: Implications for Luminescent Applications. *ACS Appl. Nano Mater.* **2019,** *2*, 5681-5687.
44. Smith, K. C.; Olafsson, A.; Hu, X.; Quillin, S. C.; Idrobo, J. C.; Collette, R.; Rack, P. D.; Camden, J. P.; Masiello, D. J. Direct Observation of Infrared Plasmonic Fano Antiresonances by a Nanoscale Electron Probe. *Phys. Rev. Lett.* **2019,** *123*, 177401.
45. Hao, F.; Sonnefraud, Y.; Dorpe, P. V.; Maier, S. A.; Halas, N. J.; Nordlander, P. Symmetry Breaking in Plasmonic Nanocavities: Subradiant LSPR Sensing and a Tunable Fano Resonance. *Nano Lett.* **2008,** *8*, 3983-3988.
46. Halas, N. J.; Lal, S.; Chang, W.-S.; Link, S.; Nordlander, P. Plasmons in Strongly Coupled Metallic Nanostructures. *Chem. Rev.* **2011,** *111*, 3913-3961.
47. Gersten, J.; Nitzan, A. Electromagnetic Theory of Enhanced Raman Scattering by Molecules Adsorbed on Rough Surfaces. *J. Chem. Phys.* **1980,** *73*, 3023-3037.
48. Hartschuh, A.; Sánchez, E. J.; Xie, X. S.; Novotny, L. High-Resolution Near-Field Raman Microscopy of Single-Walled Carbon Nanotubes. *Phys. Rev. Lett.* **2003,** *90*, 095503.
49. Schmeits, M.; Dambly, L. Fast-Electron Scattering by Bispherical Surface-Plasmon Modes. *Phys. Rev. B* **1991,** *44*, 12706-12712.
50. Tamaru, H.; Kuwata, H.; Miyazaki, H. T.; Miyano, K. Resonant Light Scattering from Individual Ag Nanoparticles and Particle Pairs. *Appl. Phys. Lett.* **2002,** *80*, 1826-1828.
51. Rechberger, W.; Hohenau, A.; Leitner, A.; Krenn, J. R.; Lamprecht, B.; Aussenegg, F. R. Optical Properties of Two Interacting Gold Nanoparticles. *Opt. Commun.* **2003,** *220*, 137-141.
52. Su, K. H.; Wei, Q. H.; Zhang, X.; Mock, J. J.; Smith, D. R.; Schultz, S. Interparticle Coupling Effects on Plasmon Resonances of Nanogold Particles. *Nano Lett.* **2003,** *3*, 1087-1090.
53. Futamata, M.; Maruyama, Y.; Ishikawa, M. Local Electric Field and Scattering Cross Section of Ag Nanoparticles under Surface Plasmon Resonance by Finite Difference Time Domain Method. *J. Phys. Chem. B* **2003,** *107*, 7607-7617.
54. Olk, P.; Renger, J.; Wenzel, M. T.; Eng, L. M. Distance Dependent Spectral Tuning of Two Coupled Metal Nanoparticles. *Nano Lett.* **2008,** *8*, 1174-1178.
55. Brown, L. V.; Sobhani, H.; Lassiter, J. B.; Nordlander, P.; Halas, N. J. Heterodimers: Plasmonic Properties of Mismatched Nanoparticle Pairs. *ACS Nano* **2010,** *4*, 819-832.

56. Schnell, M.; García-Etxarri, A.; Huber, A. J.; Crozier, K.; Aizpurua, J.; Hillenbrand, R. Controlling the near-Field Oscillations of Loaded Plasmonic Nanoantennas. *Nat. Photonics* **2009,** *3*, 287-291.
57. Kim, S.; Jin, J.; Kim, Y.-J.; Park, I.-Y.; Kim, Y.; Kim, S.-W. High-Harmonic Generation by Resonant Plasmon Field Enhancement. *Nature* **2008,** *453*, 757-760.
58. Prodan, E.; Radloff, C.; Halas, N. J.; Nordlander, P. A Hybridization Model for the Plasmon Response of Complex Nanostructures. *Science* **2003,** *302*, 419-422.
59. Prodan, E.; Nordlander, P. Plasmon Hybridization in Spherical Nanoparticles. *J Chem Phys* **2004,** *120*, 5444-5454.
60. Nordlander, P.; Oubre, C.; Prodan, E.; Li, K.; Stockman, M. I. Plasmon Hybridization in Nanoparticle Dimers. *Nano Lett.* **2004,** *4*, 899-903.
61. Wang, H.; Brandl, D. W.; Nordlander, P.; Halas, N. J. Plasmonic Nanostructures: Artificial Molecules. *Acc. Chem. Res.* **2007,** *40*, 53-62.
62. Scholl, J. A.; García-Etxarri, A.; Koh, A. L.; Dionne, J. A. Observation of Quantum Tunneling between Two Plasmonic Nanoparticles. *Nano Lett.* **2013,** *13*, 564-569.
63. Ciracì, C.; Hill, R. T.; Mock, J. J.; Urzhumov, Y.; Fernández-Domínguez, A. I.; Maier, S. A.; Pendry, J. B.; Chilkoti, A.; Smith, D. R. Probing the Ultimate Limits of Plasmonic Enhancement. *Science* **2012,** *337*, 1072-1074.
64. Toscano, G.; Raza, S.; Jauho, A.-P.; Mortensen, N. A.; Wubs, M. Modified Field Enhancement and Extinction by Plasmonic Nanowire Dimers Due to Nonlocal Response. *Opt. Express* **2012,** *20*, 4176-4188.
65. Zuloaga, J.; Prodan, E.; Nordlander, P. Quantum Description of the Plasmon Resonances of a Nanoparticle Dimer. *Nano Lett.* **2009,** *9*, 887-891.
66. Song, P.; Nordlander, P.; Gao, S. Quantum Mechanical Study of the Coupling of Plasmon Excitations to Atomic-Scale Electron Transport. *J. Chem. Phys.* **2011,** *134*, 074701.
67. Mao, L.; Li, Z.; Wu, B.; Xu, H. Effects of Quantum Tunneling in Metal Nanogap on Surface-Enhanced Raman Scattering. *Appl. Phys. Lett.* **2009,** *94*, 243102.
68. Alkan, F.; Aikens, C. M. TD-DFT and TD-DFTB Investigation of the Optical Properties and Electronic Structure of Silver Nanorods and Nanorod Dimers. *J. Phys. Chem. C* **2018,** *122*, 23639-23650.
69. Bae, G.-T.; Aikens, C. M. TDDFT and CIS Studies of Optical Properties of Dimers of Silver Tetrahedra. *J. Phys. Chem. A* **2012,** *116*, 8260-8269.
70. Chen, X.; Moore, J. E.; Zekarias, M.; Jensen, L. Atomistic Electrodynamics Simulations of Bare and Ligand-Coated Nanoparticles in the Quantum Size Regime. *Nat. Commun.* **2015,** *6*, 8921.
71. Chen, X.; Jensen, L. Morphology Dependent near-Field Response in Atomistic Plasmonic Nanocavities. *Nanoscale* **2018,** *10*, 11410-11417.
72. Liu, P.; Chulhai, D. V.; Jensen, L. Single-Molecule Imaging Using Atomistic Near-Field Tip-Enhanced Raman Spectroscopy. *ACS Nano* **2017,** *11*, 5094-5102.
73. Solis, D.; Willingham, B.; Nauert, S. L.; Slaughter, L. S.; Olson, J.; Swanglap, P.; Paul, A.; Chang, W.-S.; Link, S. Electromagnetic Energy Transport in Nanoparticle Chains Via Dark Plasmon Modes. *Nano Lett.* **2012,** *12*, 1349-1353.
74. Willingham, B.; Link, S. Energy Transport in Metal Nanoparticle Chains Via Sub-Radiant Plasmon Modes. *Opt. Express* **2011,** *19*, 6450-6461.

75. Solis, D.; Paul, A.; Olson, J.; Slaughter, L. S.; Swanglap, P.; Chang, W.-S.; Link, S. Turning the Corner: Efficient Energy Transfer in Bent Plasmonic Nanoparticle Chain Waveguides. *Nano Lett.* **2013,** *13*, 4779-4784.
76. Maier, S. A.; Kik, P. G.; Atwater, H. A. Optical Pulse Propagation in Metal Nanoparticle Chain Waveguides. *Phys. Rev. B* **2003,** *67*, 205402.
77. Hohenester, U. Quantum Corrected Model for Plasmonic Nanoparticles: A Boundary Element Method Implementation. *Phys. Rev. B* **2015,** *91*, 205436.
78. Esteban, R.; Borisov, A. G.; Nordlander, P.; Aizpurua, J. Bridging Quantum and Classical Plasmonics with a Quantum-Corrected Model. *Nat. Commun.* **2012,** *3*, 825.
79. Scholl, J. A.; Koh, A. L.; Dionne, J. A. Quantum Plasmon Resonances of Individual Metallic Nanoparticles. *Nature* **2012,** *483*, 421-427.
80. Zhu, W.; Crozier, K. B. Quantum Mechanical Limit to Plasmonic Enhancement as Observed by Surface-Enhanced Raman Scattering. *Nat. Commun.* **2014,** *5*, 5228.
81. Savage, K. J.; Hawkeye, M. M.; Esteban, R.; Borisov, A. G.; Aizpurua, J.; Baumberg, J. J. Revealing the Quantum Regime in Tunnelling Plasmonics. *Nature* **2012,** *491*, 574-577.
82. Raza, S.; Stenger, N.; Kadkhodazadeh, S.; Fischer Søren, V.; Kostesha, N.; Jauho, A.-P.; Burrows, A.; Wubs, M.; Mortensen, N. A. Blueshift of the Surface Plasmon Resonance in Silver Nanoparticles Studied with EELS. *Nanophotonics* **2013,** *2*, 131-138.
83. Prodan, E.; Car, R. Tunneling Conductance of Amine-Linked Alkyl Chains. *Nano Lett.* **2008,** *8*, 1771-1777.
84. García de Abajo, F. J. Nonlocal Effects in the Plasmons of Strongly Interacting Nanoparticles, Dimers, and Waveguides. *J. Phys. Chem. C* **2008,** *112*, 17983-17987.
85. Romero, I.; Aizpurua, J.; Bryant, G. W.; Abajo, F. J. G. d. Plasmons in Nearly Touching Metallic Nanoparticles: Singular Response in the Limit of Touching Dimers. *Opt. Express* **2006,** *14*, 9988-9999.
86. Lassiter, J. B.; Aizpurua, J.; Hernandez, L. I.; Brandl, D. W.; Romero, I.; Lal, S.; Hafner, J. H.; Nordlander, P.; Halas, N. J. Close Encounters between Two Nanoshells. *Nano Lett.* **2008,** *8*, 1212-1218.
87. Zhu, W.; Esteban, R.; Borisov, A. G.; Baumberg, J. J.; Nordlander, P.; Lezec, H. J.; Aizpurua, J.; Crozier, K. B. Quantum Mechanical Effects in Plasmonic Structures with Subnanometre Gaps. *Nat. Commun.* **2016,** *7*, 11495.
88. Alkan, F.; Aikens, C. M. Understanding Plasmon Coupling in Nanoparticle Dimers Using Molecular Orbitals and Configuration Interaction. *Phys. Chem. Chem. Phys* **2019,** *21*, 23065-23075.
89. Zhang, P.; Feist, J.; Rubio, A.; García-González, P.; García-Vidal, F. J. Ab Initio Nanoplasmonics: The Impact of Atomic Structure. *Phys. Rev. B* **2014,** *90*, 161407.
90. Alejandro, V.; Pablo, G.-G.; Johannes, F.; García-Vidal, F. J.; Angel, R. Quantum Plasmonics: From Jellium Models to Ab Initio Calculations. *Nanophotonics* **2016,** *5*, 409-426.
91. Marques, M. A. L.; Gross, E. K. U. Time-Dependent Density Functional Theory. *Annu. Rev. Phys. Chem.* **2004,** *55*, 427-455.
92. Krauter, C. M.; Bernadotte, S.; Jacob, C. R.; Pernpointner, M.; Dreuw, A. Identification of Plasmons in Molecules with Scaled Ab Initio Approaches. *J. Phys. Chem. C* **2015,** *119*, 24564-24573.

93. Bernadotte, S.; Evers, F.; Jacob, C. R. Plasmons in Molecules. *J. Phys. Chem. C* **2013,** *117*, 1863-1878.
94. te Velde, G.; Bickelhaupt, F. M.; Baerends, E. J.; Fonseca Guerra, C.; van Gisbergen, S. J. A.; Snijders, J. G.; Ziegler, T. Chemistry with ADF. *J. Comput. Chem.* **2001,** *22*, 931-967.
95. Becke, A. D. Density-Functional Exchange-Energy Approximation with Correct Asymptotic Behavior. *Phys. Rev. A* **1988,** *38*, 3098-3100.
96. Perdew, J. P. Density-Functional Approximation for the Correlation Energy of the Inhomogeneous Electron Gas. *Phys. Rev. B* **1986,** *33*, 8822-8824.
97. Perdew, J. P. Erratum: Density-Functional Approximation for the Correlation Energy of the Inhomogeneous Electron Gas. *Phys. Rev. B* **1986,** *34*, 7406-7406.
98. Lenthe, E. v.; Baerends, E. J.; Snijders, J. G. Relativistic Regular Two-Component Hamiltonians. *J. Chem. Phys.* **1993,** *99*, 4597-4610.
99. Runge, E.; Gross, E. K. U. Density-Functional Theory for Time-Dependent Systems. *Phys. Rev. Lett.* **1984,** *52*, 997-1000.
100. Casida, M. E.; Jamorski, C.; Casida, K. C.; Salahub, D. R. Molecular Excitation Energies to High-Lying Bound States from Time-Dependent Density-Functional Response Theory: Characterization and Correction of the Time-Dependent Local Density Approximation Ionization Threshold. *J. Chem. Phys.* **1998,** *108*, 4439-4449.
101. Gross, E. K. U.; Kohn, W. Local Density-Functional Theory of Frequency-Dependent Linear Response. *Phys. Rev. Lett.* **1985,** *55*, 2850-2852.
102. Casida, M. E. *Recent Advances in Density Functional Methods*; World Scientific, 1995; pp 155-192.
103. Perdew, J. P.; Burke, K.; Ernzerhof, M. Generalized Gradient Approximation Made Simple. *Phys. Rev. Lett.* **1996,** *77*, 3865-3868.
104. Jørgensen, P.; Linderberg, J. Time-Dependent Hartree–Fock Calculations in the Pariser–Parr–Pople Model. Applications to Aniline, Azulene and Pyridine. *Int. J. Quantum Chem.* **1970,** *4*, 587-602.
105. Olsen, J.; Jensen, H. J. A.; Jørgensen, P. Solution of the Large Matrix Equations Which Occur in Response Theory. *J. Comput. Phys.* **1988,** *74*, 265-282.
106. Johnson, H. E.; Aikens, C. M. Electronic Structure and TDDFT Optical Absorption Spectra of Silver Nanorods. *J. Phys. Chem. A* **2009,** *113*, 4445-4450.
107. Guidez, E. B.; Aikens, C. M. Theoretical Analysis of the Optical Excitation Spectra of Silver and Gold Nanowires. *Nanoscale* **2012,** *4*, 4190-4198.
108. López-Lozano, X.; Barron, H.; Mottet, C.; Weissker, H.-C. Aspect-Ratio- and Size-Dependent Emergence of the Surface-Plasmon Resonance in Gold Nanorods – an Ab Initio TDDFT Study. *Phys. Chem. Chem. Phys* **2014,** *16*, 1820-1823.
109. Guidez, E. B.; Aikens, C. M. Quantum Mechanical Origin of the Plasmon: From Molecular Systems to Nanoparticles. *Nanoscale* **2014,** *6*, 11512-11527.
110. Lian, K.-Y.; Sałek, P.; Jin, M.; Ding, D. Density-Functional Studies of Plasmons in Small Metal Clusters. *J. Chem. Phys.* **2009,** *130*, 174701.
111. Dreuw, A.; Weisman, J. L.; Head-Gordon, M. Long-Range Charge-Transfer Excited States in Time-Dependent Density Functional Theory Require Non-Local Exchange. *J. Chem. Phys.* **2003,** *119*, 2943-2946.

TOC Graphic